NATIONAL ADVISORY COMMITTEE
FOR AERONAUTICS

TECHNICAL NOTE 4142

EFFECTS OF LEADING-EDGE BLUNTING ON THE LOCAL HEAT

TRANSFER AND PRESSURE DISTRIBUTIONS OVER

FLAT PLATES IN SUPERSONIC FLOW

By Marcus O. Creager

Ames Aeronautical Laboratory
Moffett Field, Calif.

NACA

Washington

December 1957

NATIONAL ADVISORY COMMITTEE FOR AERONAUTICS

TECHNICAL NOTE 4142

EFFECTS OF LEADING-EDGE BLUNTING ON THE LOCAL HEAT

TRANSFER AND PRESSURE DISTRIBUTIONS OVER

FLAT PLATES IN SUPERSONIC FLOW

By Marcus O. Creager

SUMMARY

An investigation of the effect of leading-edge thickness on the flow over flat plates with square and cylindrical blunting was conducted at a Mach number of 4 and free-stream Reynolds numbers per inch of 2380 and 6600. Surface pressures were measured on a series of models whose leading-edge thicknesses ranged from 0.25 to 1 inch. Heat-transfer rates were measured from a flat plate which was blunted by a 1-inch-diameter cylindrical leading edge. All tests were performed with the instrumented surfaces at zero angle of sweep and zero angle of attack.

For the test conditions, the bow shock wave was detached and leading-edge shape had no effect on surface pressures aft of two leading-edge thicknesses. The surface pressures could be predicted by a combination of shock-wave boundary-layer interaction theory and blast wave theory. This combination applied equally well to similar data of other investigations. An empirical expression for local Reynolds number at the boundary-layer edge was found to correlate both the present data and data from other investigations covering a wide range of conditions. The local Reynolds number per inch was found to be lower than free-stream Reynolds number per inch, nearly constant for the test length, and to have negligible dependence on leading-edge bluntness. This reduction depends on the square root of the ratio of total pressures across the normal bow shock wave.

The local Nusselt number was found to depend only on the local Reynolds number for the present tests, and is predicted by the familiar Pohlhausen flat-plate theory. As compared to the sharp condition, blunting the leading edge of flat plates, with consequent reduction of local total pressure, was found to increase the heat-transfer coefficients in the region where surface static pressures were high and to reduce the coefficients where the surface static pressures approached the free-stream value.

INTRODUCTION

The presence of the boundary layer on a body effectively changes body shape. The effect on a slender body may be sufficiently large to produce a measurable strengthening or even detachment of the bow shock wave at supersonic speeds. Also, as speed is increased, interactions occur between the boundary layer and the shock wave, because the shock wave "wraps" closely back over the body. These two phenomena, shock strengthening and "wrapping" effect, change the flow field from that occurring in the usual low supersonic speed, high Reynolds number laminar flow over a plate.

A theoretical study of the hypersonic viscous flow over a sharp-nosed plate (ref. 1) brought out a parameter to describe phenomena occurring in the region of "weak" interaction between the boundary layer and the leading-edge shock wave. This interaction parameter is a special combination of the usual flow parameters, Reynolds number and Mach number. The region of strong interaction, near the leading edge, was investigated theoretically in reference 2 where this same interaction parameter was used. Correlation of surface static pressures measured on flat plates with square leading edges in hypersonic flow was obtained in reference 3 using this interaction parameter, but the magnitude of the pressures was greater than that predicted by the theories of references 1 and 2. The discrepancy between the theory and experiment was ascribed in reference 3 to leading-edge bluntness effects. Also, high static pressures measured by Kendall (ref. 4) on a flat plate with a very sharp leading edge were correlated by the interaction parameter but not satisfactorily predicted by the interaction theories of references 1 and 2.

In reference 5, Hammitt, Vas, and Bogdonoff formed an empirical relation to explain the leading-edge thickness contribution to the surface pressures measured on a series of blunted flat plates. A linear combination of the viscous interaction parameter and an empirical "inviscid" parameter was postulated. They obtained fair correlation of their own tests using this empirical relation; however, they were unable to predict the results of the experiments described by Bertram in reference 6.

More recently, blast wave theory has been applied to the inviscid problem by Lees (refs. 7 and 8) to obtain a functional relation for the inviscid pressure term. Cheng and Pallone (ref. 9), following similar lines of reasoning, obtained an inviscid pressure term similar to that of Lees. Both differ from the empirical relation of reference 5.

Lees, reference 10, analyzed the influence of the leading-edge shock wave (from blunt and sharp leading edges) on the laminar boundary layer at hypersonic speeds. For sharp leading edges he showed the effects of a highly curved attached leading-edge shock to be carried back over a large portion of the surface and to alter appreciably the temperature and vorticity at the outer edge of the boundary layer. By considering detached shocks for a blunt leading edge, Lees predicted the change of induced

pressure with interaction parameter as measured by Hammitt and Bogdonoff and described in reference 3. However, the magnitude of the pressure was not predicted.

The purpose of the research described in this paper was to study the aerodynamic and heat-transfer processes occurring over the surface aft of the leading edge of flat plates with detached shock waves. It was hoped that the results obtained with the low-density test conditions, which provide an aerodynamic magnification of the leading-edge region, would clarify the effect of size and shape of leading edge on the fundamental processes occurring there.

Experimental pressure-distribution and heat-transfer data were obtained from blunted flat plates in a rarefied gas stream. The results are compared with the results of various other similar investigations.

SYMBOLS

a exponent defined in equation (8)

b constant defined in equation (4b)

B.L.   boundary layer

c factor defined in equation (5b)

c_p specific heat at constant pressure, Btu/lb, °F

C_w constant in linear relation between viscosity and temperature

c_1 constant defined in equation (5b)

C_D drag coefficient based on frontal area

d diameter or thickness, ft

h heat-transfer coefficient, Btu/ft^2, hr, °F

I blast wave pressure term, $\dfrac{M_\infty{}^2}{(x/d)^{2/3}}$

I_0 modified Bessel function, zero order, first kind

k thermal conductivity, Btu/hr, ft^2, °F/ft

k_f film thermal conductivity, Btu/hr, ft^2, °F/ft

K constant defined by equation (8)

K_O modified Bessel function, zero order, second kind

M   Mach number, dimensionless

N   number of molecules per unit volume, 1/cu ft

Nu_x Nusselt number, $\frac{hx}{k}$, dimensionless

p   pressure, lb/sq ft

Pr   Prandtl number, $\frac{3600\ \mu c_p}{k}$, dimensionless

q   heat flow, Btu/hr

r_B outer radius of annular space around heat-transfer element, ft

r_m radius at minimum temperature point on film, ft

r   radius of point on film, ft

$Re_{\infty d}$ Reynolds number, $\frac{\rho_\infty u_\infty d}{\mu_\infty}$, dimensionless

Re_x Reynolds number, $\frac{\rho u x}{\mu}$, dimensionless

S   area defined by r_p, sq ft

t_f film thickness, ft

T   temperature, °R

T_O temperature of test-section surfaces, °R

u   velocity in x direction, ft/sec

V_m most probable molecular speed, ft/sec

x   coordinate length, ft (see fig. 3)

y   coordinate length, ft (see fig. 3)

α, β empirical constants

γ ratio of specific heats, dimensionless

δ boundary-layer thickness, ft

ζ parameter defined in equation (B9)

ϵ emissivity, dimensionless

κ Boltzmann constant, 7.28×10^{-27}, Btu/molecule, $^\circ$R

μ viscosity, lb/sec ft

ρ density, lb/cu ft

σ Stefan-Boltzmann constant, 1.73×10^{-9}, Btu/ft^2 hr, $^\circ$R^4

$\overline{\chi}$ interaction parameter, $\dfrac{M_\infty^3 \sqrt{C_w}}{\sqrt{Re_{\infty x}}}$

ω exponent of viscosity-temperature law defined in equation (B4)

Subscripts

b   blunt

d   characteristic dimension for quantity involved

p   heat-transfer element quantity

s   sharp

t_1 total quantity in free stream ahead of all disturbances

t_2 total quantity behind leading-edge normal shock wave

t_3 total quantity behind probe normal shock wave

t_δ local total quantity

w   body surface quantity

x   characteristic length for quantity involved

η "effective" recovery condition

∞ quantity evaluated at free-stream condition ahead of all disturbances

Superscript

( )'   T' method

DESCRIPTION OF EQUIPMENT AND TEST METHOD

Wind Tunnel

The tests were conducted in the Ames 8-inch low-density wind tunnel.
This wind tunnel is an open-jet nonreturn type tunnel. Air was used as
the test gas. The 8-inch tunnel is a scaled up version of the low-density
wind tunnel described in reference 11. A five-stage set of steam ejectors
is used to produce the main flow. The axisymmetric nozzle was designed
by the method described in reference 12. The nozzle was constructed of
shim stock of varying thickness and alternate shims were removed to per-
mit boundary-layer removal as described in reference 13. The design Mach
number was 4 through the stream-static pressure range of 100 to 300 microns
of mercury absolute. The boundary layer is removed by steam ejectors
operating in parallel with the main drive set. The physical arrangement
of the nozzle and test section is shown in figure 1.

Impact pressure surveys indicated that no strong shock waves were
present in the nozzle and jet when the expansion ratio across it was
properly set and controlled. Additional surveys were made in a plane
normal to the stream direction 1-1/4 inches downstream of the nozzle exit.
The static pressure of the stream was obtained by measuring the nozzle
wall pressure at a point 2 inches upstream of the exit plane of the noz-
zle. This method of obtaining stream static pressure has been described
in reference 12.

A typical Mach number distribution obtained from these measured
quantities is shown in figure 2. The Mach number was calculated in two
ways, (1) from measured impact pressure and static (wall tap) pressure
together with Rayleigh's pitot formula (circular symbols), and (2) from
measured impact pressure and upstream reservoir pressure (total head)
using the assumptions that the flow through the nozzle was isentropic and
that the probe produced a normal shock wave (square symbols). Good agree-
ment was obtained between the two methods of obtaining Mach number over
the range of pressure levels used in the investigation. Therefore, the
assumption that the flow through the nozzle was isentropic appears to be
reasonable.

Table I presents the actual usable stream diameter and Mach number
for two test-section static pressures.

Pressure Models

Four pressure models were tested. Three two-dimensional wedges
of 5° total included angle were instrumented for measurement of surface
pressures. The leading edges were cylindrical of 1, 1/2, and 1/4 inch
diameter. A 1-inch-thick slab with a square leading edge was similarly
instrumented. The models were sufficiently wide (6 in.) to span the

usable stream completely. The length of afterbody from shoulder point (tangent point) was 5 inches. Pressure orifices, 1/32-inch diameter, were installed in the upper surface at intervals of 1/16 to 1/2 inch along the midspan plane. The spacing was smallest near the leading edge. An orifice was installed at the nose of each body on the axis of symmetry.

The surface orifices were connected to a pressure manifold by stainless steel tubes. A pressure switch was used to select and connect any desired orifice to the pressure-sensing device. An oil manometer was used to measure the orifice pressures. The manometer fluid was diffusion pump oil which had been well outgassed.

Surveys were made in the flow field adjacent to the body with an impact tube. The tube end was flattened to an over-all height of about 0.030 inch to minimize disturbances in the y direction. The pressures from this probe were likewise measured with an oil-filled U-tube manometer.

Heat-Transfer Model

The heat-transfer model, figure 3, was similar in shape to the cylindrical nosed pressure distribution models described above. The model was constructed of copper with a leading-edge diameter of 1 inch. The model was 5 inches in length from the shoulder to the base. It was 6 inches wide. Cylindrical heaters installed in the body, one on each side, were used to maintain the desired model temperature.

At various locations along the model length, heat-transfer elements, hereafter called heat plugs, were installed as seen in figure 3. The heat plug is a copper spool, 1/8-inch diameter and 1/8-inch long, inserted in a hole in the model shell with a 1/64-inch air gap between the plug and the body. The spool is supported by a Bakelite stem. The surface of the plug was machined to the contour of the plate. An electrical heating coil was wound on the plug to supply heat to the plug. A differential thermocouple indicated the temperature difference between the plug and the model body. Thermocouples were mounted in the body near the heat plug to indicate temperature of the body.

A 0.003-inch-thick plastic film was placed over the surface of the model to seal the gap between the plug and the body from the air stream. The air gap was then vented to the hollow portion inside the model and thence to constant static pressure of the test chamber. Thus, the heat loss due to conduction through the air gap was minimized because of the presence of a quiescent layer of low-pressure air around the test plug.

Test Method

The heat-transfer rate from the surface of the plug to the air stream was determined as a function of the plug temperature. A test point was obtained by heating the model and the test plug to the same uniform temperature, and measuring the plug heater current for this steady-state condition.

A series of tests were made, with no air flow through the tunnel, at pressures of approximately 0.1 micron of mercury absolute and of 100 to 300 microns, to obtain the radiation and conduction heat losses. The variation of the sum of these losses with pressure was within the scatter of the data. This total loss was then treated as a tare to be subtracted from the gross heat input to the plug obtained in each test with air flow. The magnitude of the tare was approximately 10 percent of the total heat input at the highest rate and about 60 percent of the total heat input at the lowest rate. The lowest heat rate occurred near the rear of the plate at the lowest stream pressure.

At a given flow condition, net heat input to the plug was obtained at a series of plug temperature levels ranging 20° to 50° F above stagnation temperature. The net heat flow to the plug, which is the heat flow to the stream, was divided by the heat-transfer area and plotted as a function of the difference between the plug temperature and the stagnation temperature of the stream. The slope of this curve is proportional to the heat-transfer coefficient. The heat-transfer area was taken as slightly larger than the plug area as explained in Appendix A. Extrapolation of the curve to zero heat transported gives an intercept which is the difference between an "effective" recovery temperature for a uniform temperature body and stagnation temperature. A typical test curve is shown in figure 4.

The test conditions are summarized in table II. In all cases the plate leading edge was unswept, and the surface on which the measurements were made was at zero angle of attack.

EXPERIMENTAL RESULTS

Surface Pressure

The ratios of measured surface pressure to free-stream static pressure, p/p_∞, are shown in figure 5 as a function of distance x from the leading edge. Spanwise surface-pressure variations were found to be less than 2 percent within 1/2 inch of midspan. The pressures for plates with cylindrical blunting are three to four times larger than free-stream pressure near the leading edge, and decrease with distance x. It is to be noted that, in contrast, the pressures measured on the square leading-edge plate are low near the shoulder, and increase with distance x.

However, the pressure variation aft of 1-1/2 inches coincides with the distribution of the cylindrical nosed plates. The low pressures are due to overexpansion at the square leading edge and have been observed previously (refs. 5 and 14). The present results corroborate the results of references 5 and 14 that the overexpansion does not affect the pressure distribution aft of about two leading-edge thicknesses. For both types of leading edges, the pressures approach free-stream values near the rear of the bodies.

Flow-Field Surveys

Impact pressures were measured in the flow field for leading-edge Reynolds numbers of 1650 and 6600. These surveys were made to obtain an estimate of the boundary-layer thickness, flow quantities along the boundary-layer edge, and the shock-wave location.

In figure 6, the variation of impact pressure with distance above the plate is shown for a typical survey. Three distinct flow regions are evident in this figure. The first, near the surface, corresponds to the boundary layer where the impact pressure increases rapidly. A second region is observed to exist just outside the boundary layer where the impact pressure is nearly constant. The third region appears to be a region of possible shear flow where the impact pressure increases continuously with height up to the shock wave. The maximum or peak impact pressure corresponding to the shock wave is not shown in figure 6. Above the shock wave, the impact pressure drops to the free-stream value.

The height above the plate at which the peak impact pressure was measured was defined as the location of the shock wave. In figure 7, the location of the shock wave is plotted versus distance from the leading edge. Blast wave theory (refs. 7 and 9) predicts the shock-wave location for regions not too close to the leading edge of blunt flat plates in hypersonic flow to be:

$$\frac{y + (d/2)}{d} = (\text{constant}) \left(\frac{x}{d}\right)^{2/3} \tag{1}$$

This relation, adjusted to fit the data far from the cylindrical leading edge, is presented in figure 7 as the solid line. The data agree well with the prediction up to within 3 diameters from the leading edge. The constant, empirically determined, has a value of 1.47. This constant as given in reference 9 is $0.89(C_D)^{1/3}$. The value calculated from this relation for assumed C_D of 1.2 differs from the experimentally determined constant by a factor of $2^{2/3}$.

Heat Transfer

In figure 8, the local "effective" temperature recovery factor is shown plotted as a function of distance from the leading edge. The recovery factors vary from a value of about 0.65 at the shoulder to approximately values of 0.8 and 0.86 at $x/d = 2$, and are nearly constant at these values for the remainder of the plate length. It is believed that the low values at the shoulder are due to the linear extrapolation to zero heat-transfer rate as shown in figure 4 and to the implied surface condition of uniform body temperature. It is noted that the recovery factors are higher for the lower Reynolds number conditions. This may be experimental error in evaluating the recovery temperature because of the corresponding low values of heat-transfer coefficient.

The measured heat-transfer coefficients are plotted as a function of x/d as shown in figure 9. The heat-transfer coefficients are high near the leading edge and decrease with distance from the leading edge. It is also noted that the heat-transfer coefficients increase with increase in free-stream Reynolds number based on leading-edge thickness.

DISCUSSION

Boundary-Layer Thickness

The edge of the boundary layer was determined from the velocity distributions through the boundary layer. The velocities were computed from the impact pressures on the assumption that the total temperature was constant through the flow field and the static pressure gradient normal to the plate was equal to zero. The edge of the boundary layer is defined as that distance above the plate surface where the velocity ratio has approached within 1 percent of the straight "reference" line drawn through the experimental points in region II, see figure 10.

The resultant boundary-layer thicknesses are presented in figure 11. The theoretical prediction of boundary-layer thickness on a flat plate with zero thickness leading edge, reference 1, as altered by introduction of the leading-edge thickness, d, is given below:

$$\frac{\delta}{d} = \left[\frac{1.73}{M_\infty^2} \left(\frac{T_w}{T_\infty} \right) + 0.332(\gamma - 1) + \frac{4.27}{M_\infty^2} \right] \frac{M_\infty^2 \sqrt{C_w}}{\sqrt{Re_{\infty d}}} \sqrt{\frac{x}{d}} \qquad (2)$$

Equation (2) is compared with two sets of data in figure 11 for cylindrical blunting. It is noted that the boundary-layer thickness for the thin leading-edge plate is predicted fairly well by equation (2), except for

the region near the leading edge. The boundary-layer thickness measured over the thick leading-edge plate is somewhat lower than predicted by the theory.

Surface Pressure Distribution

References 5 and 6 indicate that a linear combination of a viscous term and an inviscid term may be the proper type of formulation to describe the surface pressure distribution over blunt flat plates in hypersonic flow. The following linear combination of pressure terms is proposed:

$$\frac{p}{p_\infty} = 1 + \alpha b\overline{X} + \beta cI \tag{3}$$

where α and β are empirical constants to be determined by comparison with experiment.

The viscous pressure term, $b\overline{X}$, is the parameter pointed out in reference 1 as a result of the theoretical study of hypersonic flow over a flat plate with a zero thickness leading edge, where,

$$\overline{X} = \frac{M_\infty^3 \sqrt{C_W}}{\sqrt{Re_{\infty X}}} \tag{4a}$$

$$b = \left[\frac{0.865}{M_\infty^2}\left(\frac{T_W}{T_\infty}\right) + 0.166(\gamma-1)\right]\gamma \tag{4b}$$

$$C_W = \frac{\mu_W}{\mu_\infty}\frac{T_\infty}{T_W} \tag{4c}$$

The inviscid pressure term, cI, is obtained from the blast wave analogy to the hypersonic flow over blunt flat plates, references 7 and 8, and also from a characteristic development of the flow field described briefly in reference 9, where

$$I = \frac{M_\infty^2}{\left(\frac{x}{d}\right)^{2/3}} \tag{5a}$$

The factor c in the inviscid pressure term, as explained in references 8 and 9, is proportional to the energy released into the transverse flow

field by the blunt leading edge. The more exact formulation of this factor, reference 9, is given as

$$c = c_1(C_D)^{2/3} \qquad (5b)$$

The value of c_1 in the above equation is given in reference 9 as 0.112 for air and 0.169 for helium. The pressure drag coefficient, C_D, for the cylindrical leading edge is approximately 1.2 (see, e.g., ref. 9). For a square leading edge the drag coefficient is found to be approximately 1.8 if one assumes impact pressure acting over the complete front face.

A correlation of the surface pressures on flat plates in supersonic and hypersonic flow is shown in figure 12 where measured pressures are compared with values obtained from the following form of equation (3):

$$\frac{p}{p_\infty} = 1 + \frac{b\overline{X}}{\sqrt{C_W}} + \frac{cI}{2^{2/3}} \qquad (6)$$

It has been found by trial that values of $1/\sqrt{C_W}$ for α and $1/2^{2/3}$ for β result in the best correlation of the data of the present tests, as well as data from references 4, 5, 6, 15, and 16, see table III. The solid line represents a 1-to-1 correspondence of measured to theoretical values. The data are noted to be within approximately 20 percent of the solid (theoretical) line. The calculation has been made for a temperature recovery factor assumed equal to 0.86 for the data of references 4, 5, and the present tests. The recovery factor for the helium data of reference 5 was assumed to be 0.82. Calculations for the conditions of references 15 and 16 were made using their measured wall temperatures. The wall temperature affects the parameter b and C_W of the viscous term in equation (6). In view of the considerable range of variables encompassed by this correlation, the semiempirical expression in equation (6) is believed to be quite general in applicability.

Local Mach Number

The local Mach number along the boundary-layer edge was obtained by two methods which are compared in figure 13. Both methods utilize the measured surface pressures and the assumption of zero pressure gradient normal to the plate. The set of points in figure 13 labeled "local measurements" was obtained by use of local measured impact pressures. The second set, labeled "reduced total pressure," was obtained by assuming the total pressure along the boundary-layer edge to be constant and equal to the total pressure behind the leading-edge normal shock wave.

Two results are noted from figure 13. First, although the Mach number
is seen to increase slowly with distance from the nose, it does not
reach free-stream Mach number within the test length. The second and
more important result is the excellent agreement between the Mach number
distributions obtained by the two different methods.

Reduced local Mach numbers have been reported previously by Brinich
(ref. 17) as obtained in tests conducted at a Mach number of 3.1 over a
hollow cylinder. Both sharp and square leading edges were tested, and
the local Mach number was found to be reduced up to a distance of approx-
imately 3000 nose thicknesses back from the leading edge. Also, Crawford
and McCauley have reported (ref. 18) reduced local Mach numbers obtained
over a hemispherical-nosed cylinder at free-stream Mach number of 6.8 for
distances up to 3 nose thicknesses back along the afterbody.

From the results of the present tests and those of references 17
and 18, it can be concluded that the local properties along the boundary-
layer edge can be obtained by the reduced total pressure method for the
range of the present tests and for similar tests of other investigations,
if a detached normal shock exists at the leading edge.

Local Reynolds Number

The assumption that the total pressure was reduced and constant
along the boundary-layer edge was applied to the present data, and the
local Reynolds numbers were computed along the boundary-layer edge. In
figure 14 the ratio $Re_x/Re_{\infty d}$ is shown plotted as a function of dimen-
sionless distance, x/d. The quantity Re_x is based on local quantities
at the edge of the boundary layer and distance x. The quantity $Re_{\infty d}$
is based on free-stream conditions ahead of the leading-edge shock wave
and the diameter of the leading edge. The data are linear on the loga-
rithmic plot. The best fit to the data, determined by method of least
squares, resulted in the relation

$$\frac{Re_x}{Re_{\infty d}} = 0.41 \left(\frac{x}{d}\right)^{0.91} \tag{7}$$

This empirical relation is shown as the solid line in figure 14. It is
noted that the local Reynolds number at the boundary-layer edge is
decreased to about 40 percent of the free-stream value and this percent-
age decrease does not vary for changes of 10 to 1 in leading-edge Reynolds
numbers. Reduction in local Reynolds number has also been obtained by
Brinich (ref. 17) in his transition studies.

In view of the successful correlation of the present data in terms
of local Reynolds number, the method described above was applied to the
results of Kendall (ref. 4), Hammitt, Vas, and Bogdonoff (ref. 5), Bertram
(refs. 6 and 15), and Erickson (ref. 16). The results are presented in
figure 15. The solid line represents a datum line or variation where the
local Reynolds number per inch is equal to free-stream Reynolds number
per inch. It may be noted that in figure 15 the effects of leading-edge
thickness and free-stream Reynolds number, for each set of points, are
fully accounted for. Also in figure 15 the Reynolds number ratio for a
fixed value of x/d decreases with increasing Mach number and seems to
approach a limiting value as Mach number increases. There are two other
parameters which differ among these sets of data, namely, leading-edge
shape and test gas. In the previous section on surface pressures, the
shape of the leading edge has been shown not to affect the surface pres-
sure distribution past an x/d of 1 to 2. Thus we may rule out the
leading-edge shape parameter provided a detached shock exists, leaving
Mach number and ratio of specific heats as possible parameters affecting
correlation of the sets of data.

The empirical fit to each set of data in figure 15 was found by the
method of least squares. The general relationship is represented by the
following equation.

$$\frac{\mathrm{Re}_x}{\mathrm{Re}_{\infty d}} = K \left(\frac{x}{d}\right)^a \tag{8}$$

The values of K and a are tabulated in table IV together with those
for the present tests.

The slope is practically the same for all the sets of data shown
in figure 15. Thus the test gas and Mach number dependence is contained
in the parameter K of equation (8). An analysis presented in Appendix B
suggests a correlation parameter, namely, the total pressure ratio across
the normal shock occurring at free-stream Mach number. Thus the values
of the parameter K were plotted versus the total pressure ratio across
the normal shock as shown in figure 16. It is noted that the parameter K
is correlated well by the following equation.

$$K = 1.2 \left(\frac{p_{t_2}}{p_{t_1}}\right)^{1/2} \tag{9}$$

An average value of the slope, a, was taken to be 0.91. This average
value of a and the relation for K in equation (9) when substituted
in equation (8) give the best fit to all the data sets.

$$\frac{Re_x}{Re_{\infty d}} = 1.2 \left(\frac{p_{t_2}}{p_{t_1}} \right)^{1/2} \left(\frac{x}{d} \right)^{0.91} \tag{10}$$

The excellent correlation obtained by the use of equation (10) is shown in figure 17. It should be noted that the data correlated by use of equation (10) cover an extremely wide range of variables. For example, the data include a Mach number range of from 4 to 17.3, leading-edge thicknesses of 0.0002 to 1.0 inch, and free-stream Reynolds numbers per inch from 2500 to 10^6. In addition, the data include tests both in air and in helium. The success of this correlation suggests that in all cases considered the total pressure along the boundary-layer edge is constant and equal to the total pressure behind the leading-edge normal shock. Further tests are required to determine the applicability of the correlation over ranges of variables beyond those covered by the data shown.

Heat Transfer

The heat-transfer coefficients are presented in dimensionless form in figure 18 where the local Nusselt number is plotted as a function of the local Reynolds number. The well-known Pohlhausen solution for local heat transfer in the laminar boundary layer over a flat plate is

$$Nu_x = 0.332(Pr)^{1/3} \sqrt{Re_x} \tag{11}$$

Because the Prandtl number of the present tests is nearly 0.72, equation (11) reduces to

$$Nu_x = 0.295 \sqrt{Re_x} \tag{12}$$

It is to be noted in figure 18 that this simple Pohlhausen solution fits the majority of the data quite well. The scatter from the line of equation (12) can be explained by the limitations of the present heat-transfer instrumentation. The heat-transfer elements yield inaccurate results when h falls to values of around 0.5 Btu/ft^2, hr, °F. The tare then becomes equal or greater than the net heat transfer to the stream.

The effect of blunting on the heat-transfer coefficients over a flat plate can now be examined. The correlation of figure 18 was made on the basis of properties evaluated at local conditions at the edge of the boundary layer. However, in order to account for nonlinear variation of viscosity and thermal conductivity, the well-known T' method

(ref. 19) for evaluating properties was incorporated. As shown in Appendix C, the ratio of heat-transfer coefficients for blunt and sharp plates is

$$\frac{h_b{'}}{h_s{'}} = \frac{\left(k' \sqrt{\dfrac{T\mu}{T'\mu'}} \right)_b}{\left(k' \sqrt{\dfrac{T\mu}{T'\mu'}} \right)_\infty} \sqrt{\frac{Re_x}{Re_{\infty d}}} \sqrt{\frac{d}{x}} \qquad (13)$$

Note that the ratio of Reynolds numbers appearing under the square root in equation (13) can be obtained directly from the present correlation as given by equation (10). The primed quantities are evaluated from the equations of Appendixes B and C and the known pressure distribution over the surface of the blunted plate. The quantities applying to the sharp plate are evaluated from free-stream conditions.

The results are now applied to a flat plate in flight for the following set of assumed conditions:

$$M_\infty = 10$$

$$Re_\infty/ft = 10^6$$

$$T_\infty = 420^\circ \ R$$

$$T_w = 1000^\circ \ R$$

$$d = 1 \ in.$$

The reduced total pressure is assumed to persist over the entire surface. The local static pressure and local Mach number distributions are presented in figures 19 and 20 for these conditions. The pressure was calculated by equation (3), and the local Mach number was calculated from equation (B5). The ratio of the heat-transfer coefficients for a blunted plate to the heat-transfer coefficients for a sharp plate was calculated by equation (13). The variation of this calculated ratio with distance from the leading edge is shown in figure 21.

It is noted from figures 19, 20, and 21 that the effect of blunting the leading edge is to increase the heat-transfer coefficients in the region over the plate surface where high static pressures exist. However, as noted from figure 21, the effect of blunting the leading edge is to reduce the heat-transfer coefficient far back on the plate, where surface pressures have a value near that of the free stream. It is thus concluded that blunting with consequent reduction of total pressure along the boundary-layer edge increases the heat-transfer coefficient near the

leading edge where the high static pressures exist, and reduces the heat-transfer coefficient far back on the plate where the static surface pressure approaches the free-stream value.

SUMMARY OF RESULTS

Pressures and heat-transfer rates were measured on blunt flat plates at a nominal Mach number of 4 for free-stream Reynolds numbers per inch of 2380 and 6600 in air. The Reynolds number based on leading-edge thickness ranged from 600 to 6600. Surface pressures near the leading edge were found to be nearly three to four times larger than free-stream static pressures, and these higher pressures persisted far back on the plates. A linear combination of the viscous hypersonic parameter and the blast wave inviscid parameter was found to correlate pressure distributions obtained in this and other investigations for Mach numbers of 4 to 17.3, free-stream Reynolds numbers per inch from 2500 to 10^6, and leading-edge thicknesses from 0.0002 to 1.0 inch.

Boundary-layer thicknesses, obtained for leading-edge Reynolds number of 1650 and 6600, agreed with the theory for flat plates with zero thickness leading edge. Experimentally determined flow quantities along the boundary-layer edge agreed remarkably well with values calculated with the assumption of reduced total pressure equal to the leading-edge stagnation pressure.

The local Reynolds number at the boundary-layer edge was found to be decreased to about 40 percent of the free-stream value by blunting at a Mach number of 4. The decrease in local Reynolds number was not appreciably affected by changes of 10 to 1 in leading-edge Reynolds number.

A general correlation of the ratio of local Reynolds number to leading-edge Reynolds number was obtained by comparing the present test results with the results of similar tests which covered wide ranges of Mach number, leading-edge thickness, free-stream Reynolds number, and test gas. The basic assumption underlying this correlation is that the total pressure along the boundary-layer edge does not differ appreciably from stagnation point pressure. If this condition is assumed to be true, then the local Reynolds number along the boundary-layer edge is lower than free-stream Reynolds number by a factor which is very nearly the square root of the total pressure ratio across the normal shock wave at the leading edge.

Heat-transfer rates were measured for leading-edge Reynolds numbers of 2380 and 6600. Local Nusselt numbers were correlated by local Reynolds numbers and predicted by the well-known Pohlhausen solution wherein local conditions at the boundary-layer edge are used. As compared to the sharp condition, blunting of a flat plate was found to increase the heat-transfer coefficients in the region near the leading edge where high static

pressures and reduced total pressure exist, and to decrease the heat-
transfer coefficients in the region far from the leading edge where
reduced static and total pressures exist.

Ames Aeronautical Laboratory
    National Advisory Committee for Aeronautics
   Moffett Field, Calif., Aug. 9, 1957

APPENDIX A

DETERMINATION OF THE HEAT-TRANSFER AREA

The net heat was considered to be transferred from the top surface of the cylindrical test plug to the air stream. Thus the area, S, used in the following equation was the area of the top of the test plug.

$$q = hS(T-T_\eta) \qquad\qquad (A1)$$

However, the film stretched over the model (see fig. 3 insert) does conduct some heat away from the plug. Also, the film receives energy from the cylindrical surface of the plug by free molecular conduction through the annular air space around the plug. This film acts much as a circular fin in dissipating the heat from the test plug. This effect is to increase the area to be used in calculating the heat-transfer coefficient. The following analysis of the fin effect leads to a form of the correction to the test area.

The differential equation governing the temperature distribution in the circular film fin may be found by summing the quantities of heat transferred by the various means to and from an annular element of the fin (see sketch (a)). Azimuthal variations of these quantities around the test plug will be considered negligible. The assumption is made that temperature differences are small, so that the radiation exchange terms may be written in linear form. The width of the annular air space is of the order of a mean free path of the gas. Thus, it is assumed that the annular element of fin gains heat from the plug by free molecular conduction through the annular air space. This element also transfers heat to the stream by convection through the flow boundary layer. A further assumption will be made that the variation of heat-transfer coefficient and recovery temperature is negligible over the area of film considered. When these terms are combined with the normal terms of conduction in the film fin, the heat flow balance may be written for the annular element
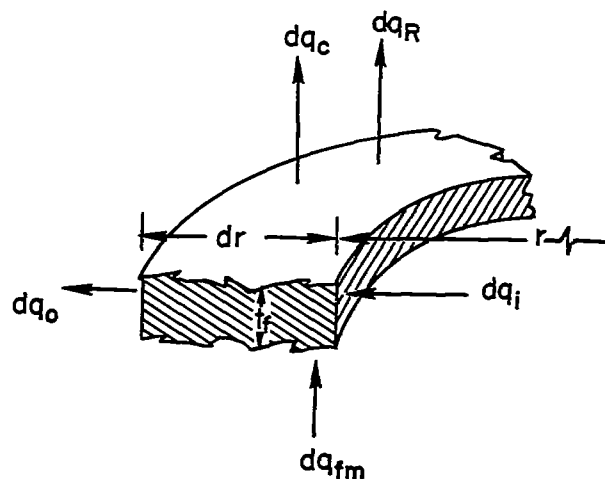
Sketch (a)

$$dq_0 + dq_c + dq_R - dq_i - dq_{fm} = 0$$

where

dq_o heat flow out of element by film conduction

dq_c heat flow from element by air-stream conduction

dq_R heat flow from element by radiation

dq_i heat flow into element by film conduction

dq_{fm} heat flow to lower side of element by free molecular conduction

The differential equation is then found to be:

$$\frac{d^2}{dr^2}\left(T - \frac{A}{B}\right) + \frac{1}{r}\frac{d}{dr}\left(T - \frac{A}{B}\right) - B\left(T - \frac{A}{B}\right) = 0 \tag{A2}$$

The differential equation (A2) is a form of Bessel's equation. The solution may be written in terms of modified Bessel functions of zero order, first and second kinds, as

$$T - \frac{A}{B} = A_3 I_0(r\sqrt{B}) + A_4 K_0(r\sqrt{B}) \tag{A3}$$

where

$$A \equiv \frac{T_p}{t_f k_f}\left(\frac{3NV_m \kappa}{2\sqrt{\pi}} + 4\sigma\epsilon T_o^3\frac{T_o}{T_p} + h\frac{T_\eta}{T_p}\right) \tag{A4}$$

$$B \equiv \frac{1}{t_f k_f}\left(\frac{3NV_m \kappa}{2\sqrt{\pi}} + 4\sigma\epsilon T_o^3 + h\right) \tag{A5}$$

and A_3 and A_4 are constants of integration to be determined by the following boundary conditions at

$$\left.\begin{array}{ll} r = r_p , & T = T_p \\[2mm] r = r_w , & T = T_w = T_p \end{array}\right\} \tag{A6}$$

In the range of interest, the modified Bessel functions in the solution (A3) may be replaced by the asymptotic expressions, reference 20, for large values of the argument $(r \sqrt{B})$. These expressions are

$$\left. \begin{aligned} I_0(r \sqrt{B}) &\cong \frac{\exp(r \sqrt{B})}{\sqrt{2\pi(r \sqrt{B})}} \\[2em] K_0(r \sqrt{B}) &\cong \sqrt{\frac{\pi}{2(r \sqrt{B})}} \; \exp(-r \sqrt{B}) \end{aligned} \right\} \tag{A7}$$

Relations (A7) are introduced into equation (A3), the boundary conditions are applied, and the constants of integration are evaluated. The radius, r_m, at which the minimum temperature occurs is found to be very nearly the average radius given by

$$r_m = \frac{r_w + r_p}{2} \tag{A8}$$

The temperature distribution in the circular fin is then given by the resulting form of equation (A3) as

$$\frac{T - \frac{A}{B}}{T_p - \frac{A}{B}} = \sqrt{\frac{r_p}{r_m}} \left[\frac{\exp(r \sqrt{B}) + \left(\dfrac{2r_m \sqrt{B}-1}{2r_m \sqrt{B}+1} \right) \exp(2r_m \sqrt{B}-r \sqrt{B})}{\exp(r_p \sqrt{B}) + \left(\dfrac{2r_m \sqrt{B}-1}{2r_m \sqrt{B}+1} \right) \exp(2r_m \sqrt{B}-r_p \sqrt{B})} \right] \tag{A9}$$

The heat removed from the plug by the film is transferred to the stream according to the following relation

$$dq = h(T-T_\eta)dS \tag{A10}$$

This expression is integrated using the temperature distribution in equation (A9) for T, and assuming a constant heat-transfer coefficient. The resulting expression is found

$$q = 2\pi h \int_{r_p}^{r_m} (T-T_\eta) r \; dr \tag{A11}$$

Assuming that the amount of heat represented in equation (A11) were to be transferred at plug temperature from an area given by $\pi \bar{r}^2$, we have

$$q = \pi h (\bar{r}^2 - r_p^2)(T_p - T_\eta) \tag{A12}$$

Thus by equating the right-hand sides of equations (A11) and (A12) we can express the heat-transfer radius $\bar{r}$ as follows:

$$\bar{r}^2 = r_p^2 + \frac{r_p^2}{1-(T_\eta/T_p)} \left[2 \int_1^{\frac{r_m}{r_p}} \left(\frac{r}{r_p}\right)\left(\frac{T}{T_p}\right) d\left(\frac{r}{r_p}\right) - \frac{T_\eta}{T_p}\left(\frac{r_m^2}{r_p^2} - 1\right) \right] \tag{A13}$$

In actual computation of the correction, the emissivity of the film was assumed to be the same as that of the chrome-plated plug surface, that is 0.1. The emissivity of the plug with film was found to check closely with the value normally taken for polished chrome. The conductivity of the film was taken as 0.1 Btu/hr, ft^2, °F/ft. This value was obtained from manufacturer's literature, and was not checked experimentally during these tests. The first approximation to h, found by using r_p, was used to determine $\bar{r}$. The correct heat-transfer coefficient is then found using this $\bar{r}$ computed from equation (A13).

APPENDIX B

LOCAL REYNOLDS NUMBERS

The ratio of local to free-stream Reynolds number is analyzed for the case of a blunt flat plate in supersonic flow. The general assumption is made that the total pressure along the boundary-layer edge is lower than the total pressure in the free stream ahead of the bow shock wave. In addition, the static pressure is assumed constant through the boundary layer. The local Mach number at the boundary-layer edge is specified by the local static and total pressures. The local static temperature can be found from the local Mach number and the known stagnation conditions.

The defining expression for the ratio of Reynolds numbers is given below.

$$\frac{Re_x}{Re_{\infty d}} = \left(\frac{p}{p_\infty}\right)\left(\frac{M}{M_\infty}\right)\left(\frac{T_\infty}{T}\right)^{1/2}\left(\frac{\mu_\infty}{\mu}\right)\left(\frac{x}{d}\right) \tag{B1}$$

In order to relate the various terms in equation (B1) to the ratio of local static to total pressure, the following equations are obtained from reference 21.

$$\frac{p}{p_{t_\delta}} = \left(1 + \frac{\gamma-1}{2} M^2\right)^{-\frac{\gamma}{\gamma-1}} \tag{B2}$$

$$\frac{T}{T_{t_\delta}} = \left(1 + \frac{\gamma-1}{2} M^2\right)^{-1} \tag{B3}$$

The viscosity is assumed to vary as a power of the absolute temperature

$$\mu \sim (T)^\omega \tag{B4}$$

The following ratios are easily obtained from equations (B2), (B3), and (B4).

$$\frac{M}{M_\infty} = \left[\frac{1-(T/T_{t_\delta})}{1-(T_\infty/T_{t_\delta})}\right]^{1/2} \left(\frac{p_\infty}{p}\frac{p_{t_\delta}}{p_{t_1}}\right)^{\frac{\gamma-1}{2\gamma}} \tag{B5}$$

$$\frac{T_\infty}{T} = \left(\frac{p_\infty}{p}\frac{p_{t_\delta}}{p_{t_1}}\right)^{\frac{\gamma-1}{\gamma}} \tag{B6}$$

$$\frac{\mu_\infty}{\mu} = \left(\frac{p_\infty}{p}\frac{p_{t_\delta}}{p_{t_1}}\right)^{\frac{\gamma-1}{\gamma}\omega} \tag{B7}$$

The ratios as determined in equations (B5), (B6), and (B7) are introduced into equation (B1). The resulting expression is

$$\frac{Re_x}{Re_{\infty d}} = \left(\frac{p_{t_\delta}}{p_{t_1}}\right)^\zeta \left(\frac{p}{p_\infty}\right)^{1-\zeta} \left[\frac{1-(T/T_{t_\delta})}{1-(T_\infty/T_{t_\delta})}\right]^{1/2} \left(\frac{x}{d}\right) \tag{B8}$$

where the constant ζ is as follows:

$$\zeta = \left(\frac{\gamma-1}{\gamma}\right)(1+\omega) \tag{B9}$$

If the assumption is made that the local total pressure is reduced to that value of total pressure existing behind the leading-edge normal shock, the ratio of Reynolds numbers becomes,

$$\frac{Re_x}{Re_{\infty d}} = \left(\frac{p_{t_2}}{p_{t_1}}\right)^\zeta \left\{\left(\frac{p}{p_\infty}\right)^{1-\zeta} \left[\frac{1-(T/T_{t_1})}{1-(T_\infty/T_{t_1})}\right]^{1/2}\right\} \left(\frac{x}{d}\right) \tag{B10}$$

The total pressure ratio term is a function only of free-stream Mach number and gas. As is shown in the correlations of figure 15, the braced term is constant for fixed free-stream Mach number.

Probable values of the exponent ζ may be calculated. For a temperature range from 300° R to 900° R in air, ω is nearly 0.75. From equation (B9) the value of ζ is found to be 0.5. For helium, ω is approximately 0.63 for a temperature range of 10° to 100° R, and ζ is found to be 0.65.

APPENDIX C

REFERENCE TEMPERATURE FOR FLUID PROPERTIES

The temperature at which fluid properties are evaluated is arbitrary in empirical correlations. In reference 19 an expression is obtained which gives an evaluation temperature, the well-known T' temperature. The advantage of the use of the T' temperature is that when properties are evaluated in this manner, the drag and heat transfer can be expressed in such a form as to minimize their dependence on Mach number, wall temperature, Prandtl number, and power law exponent for viscosity and thermal conductivity. The expression derived in reference 19 is presented below.

$$\frac{T'}{T} = 1 + 0.032 \ M^2 + 0.58 \left(\frac{T_w}{T} - 1\right) \tag{C1}$$

If the Nusselt number, as given by the normal Pohlhausen solution, is written in terms of the T' properties, the form can be shown to be,

$$h' = \left(k' \sqrt{\frac{T\mu}{T'\mu'}}\right)\left(\frac{0.295 \ \sqrt{Re_x}}{x}\right) \tag{C2}$$

It may be noted from equation (C2) that the T' method of obtaining reference temperature merely takes into account the nonlinearity of the viscosity and thermal conductivity variation with temperature. Thus, if an experiment is conducted over a range of temperatures where the viscosity and conductivity vary linearly with temperature, results obtained for heat-transfer correlation will be unaltered by the T' method of data reduction.

For the case of blunt leading edges, the properties are evaluated at local conditions, the T' method is applied to the local temperatures, and equation (C2) becomes:

$$h_b' = \left(k' \sqrt{\frac{T\mu}{T'\mu'}}\right)_b\left(\frac{0.295 \ \sqrt{Re_x}}{x}\right) \tag{C3}$$

For the case of the sharp leading edge, the local properties are normally considered as based on free-stream conditions ahead of all disturbances, and the T' method is applied as follows:

$$h_s{}' = \left(k' \sqrt{\frac{T\mu}{T'\mu'}}\right)_\infty \left(\frac{0.295 \sqrt{Re_{\infty x}}}{x}\right) \tag{C4}$$

The following ratio of heat-transfer coefficient is obtained from equations (C3) and (C4).

$$\frac{h_b{}'}{h_s{}'} = \frac{\left(k' \sqrt{\frac{T\mu}{T'\mu'}}\right)_b}{\left(k' \sqrt{\frac{T\mu}{T'\mu'}}\right)_\infty} \sqrt{\frac{Re_x}{Re_{\infty x}}} \tag{C5}$$

REFERENCES

1. Lees, Lester, and Probstein, Ronald F.: Hypersonic Viscous Flow
   Over a Flat Plate. Princeton University, Aero. Eng. Lab. Rep.
   No. 195, Apr. 20, 1952.

2. Lees, Lester: On the Boundary Layer Equations in Hypersonic Flow
   and Their Approximate Solution. Princeton University, Aero. Eng.
   Lab. Rep. No. 212, Sept. 20, 1952.

3. Hammitt, A. G., and Bogdonoff, S. M.: A Study of the Flow about
   Simple Bodies at Mach Numbers from 11 to 15. Princeton University,
   Aero. Eng. Lab. Rep. No. 277, Sept. 1954. (Also pub. as WADC
   TR 54-257, Oct. 1954)

4. Kendall, James M., Jr.: Experimental Investigation of Leading Edge
   Shock Wave - Boundary Layer Interaction at Hypersonic Speeds.
   I.A.S. Preprint No. 611, 1956. (Also pub. as GALCIT Memo. No. 30)

5. Hammitt, A. G., Vas, I. E., and Bogdonoff, S. M.: Leading Edge
   Effects on the Flow over a Flat Plate at Hypersonic Speeds.
   Princeton University, Aero. Eng. Lab. Rep. No. 326, Sept. 1955.

6. Bertram, Mitchel H.: Viscous and Leading-Edge Thickness Effects on
   the Pressures on the Surface of a Flat Plate in Hypersonic Flow.
   Jour. Aero. Sci., vol. 21, no. 6, June 1954, pp. 430-431.

7. Lees, Lester: Inviscid Hypersonic Flow over Blunt-Nosed Slender
   Bodies. GALCIT Memo. No. 31, Feb. 1, 1956.

8. Lees, Lester, and Kubota, Toshi: Inviscid Hypersonic Flow over
   Blunt-Nosed Slender Bodies. Jour. Aero. Sci., vol. 24, no. 3,
   Mar. 1957, pp. 195-202.

9. Cheng, H. K., and Pallone, A. J.: Inviscid Leading-Edge Effect in
   Hypersonic Flow. Jour. Aero. Sci., vol. 23, no. 7, July 1956,
   pp. 700-702.

10. Lees, Lester: Influence of Leading-Edge Shock Wave on the Laminar
    Boundary Layer at Hypersonic Speeds. Jour. Aero. Sci., vol. 23,
    no. 6, June 1956, pp. 594-600.

11. Stalder, Jackson R., Goodwin, Glen, and Creager, Marcus O.: A Com-
    parison of Theory and Experiment for High-Speed Free-Molecule Flow.
    NACA Rep. 1032, 1951.

12. Owen, J. M., and Sherman, F. S.: Design and Testing of a Mach 4
    Axially Symmetric Nozzle for Rarified Gas Flows. Univ. of Calif.,
    Inst. of Eng. Res. Rep. HE-150-104, July 23, 1952.

13. Stalder, Jackson R., Goodwin, Glen, and Creager, Marcus O.: Heat Transfer to Bodies in a High-Speed Rarified-Gas Stream. NACA Rep. 1093, 1952.

14. Holder, D. W., and Chinneck, A.: The Flow Past Elliptic-Nosed Cylinders and Bodies of Revolution in Supersonic Air Streams. The Aero. Quart., vol. IV, part IV, Feb. 1954, pp. 317-340.

15. Bertram, Mitchel H.: Boundary-Layer Displacement Effects in Air at Mach Numbers of 6.86 and 9.6. NACA TN 4133, 1957.

16. Erickson, Wayne: A Pressure Distribution Study of Some Simple Sharp Nosed Models at Mach Numbers of 16 to 18 in Helium Flow. NACA TN 4113, 1957.

17. Brinich, Paul F.: Effect of Leading-Edge Geometry on Boundary-Layer Transition at Mach 3.1. NACA TN 3659, 1956.

18. Crawford, Davis H., and McCauley, William D.: Investigation of the Laminar Aerodynamic Heat-Transfer Characteristics of a Hemisphere-Cylinder in the Langley 11-Inch Hypersonic Tunnel at a Mach Number of 6.8. NACA TN 3706, 1956.

19. Rubesin, M. W., and Johnson, H. A.: A Critical Review of Skin-Friction and Heat-Transfer Solutions of the Laminar Boundary Layer of a Flat Plate. Trans. ASME, vol. 71, no. 4, May 1949, pp. 383-388.

20. von Kármán, Theodore, and Biot, Maurice A.: Mathematical Methods in Engineering. First ed., McGraw-Hill Book Co., Inc., New York, N.Y., 1940, p. 62.

21. Ames Research Staff: Equation, Tables, and Charts for Compressible Flow. NACA Rep. 1135, 1953.

TABLE I.- STREAM CONDITIONS

Static pressure, microns Hg abs	Mach number	Stream diameter, in.
300	3.95	3.6
100	3.87	3.0

TABLE II.- SUMMARY OF PRESENT TEST CONDITIONS

Type of test	Model leading edge		Test conditions		Figures showing data
	Thickness, in.	Shape	M_∞	$Re_\infty/in.$	
Surface pressure	1/4	Cylindrical	3.95	6600	5,12,14,15,17
	1/2	↓	↓	↓	
	1				
	1	Square			
	1/4	Cylindrical	3.87	2380	
	1/2				
	1	↓			
	1	Square	↓	↓	↓
Local flow field	1/4	Cylindrical	3.95	6600	7,11,13
	1	↓	↓	↓	6,7,10,11,13
Heat-transfer and recovery factor	↓	↓	3.95	6600	8,9,18
			3.87	2380	↓

TABLE III.- TEST CONDITIONS OF OTHER INVESTIGATIONS

Investigation	$Re_{\infty d}$	M_∞	Gas	Leading edge
Kendall (ref. 4)	12 to 50	5.8	Air	Sharp
Bertram (ref. 6)	370 to 1900	6.86	Air	Square
Bertram (ref. 15)	38 to 55	9.6	Air	Sharp
Hammitt and Bogdonoff (ref. 3)	3480 to 6100	11.8	Helium	Square
Hammitt, Vas, and Bogdonoff (ref. 5)	15,000 to 38,000	12.7	Helium	Square
Erickson (ref. 16)	650 and 685	16 and 17.3	Helium	Sharp

TABLE IV.- REYNOLDS NUMBER CORRELATION PARAMETERS

Investigation	M_∞	γ	K	a
Present tests	3.95	1.4	0.415	0.91
Kendall (ref. 4)	5.8	1.4	.223	.95
Bertram (ref. 6)	6.86	1.4	.152	.93
Bertram (ref. 15)	9.6	1.4	.117	.87
Hammitt and Bogdonoff (ref. 3)	11.8	1.67	.129	.89
Hammitt, Vas, and Bogdonoff (ref. 5)	12.7	1.67	.132	.88
Erickson (ref. 16)	16	1.67	.096	.90
Erickson (ref. 16)	17.3	1.67	.076	.93

To boundary-layer removal ejectors

Valve

Upstream reservoir

Nozzle

Test section

To main ejectors

Air in
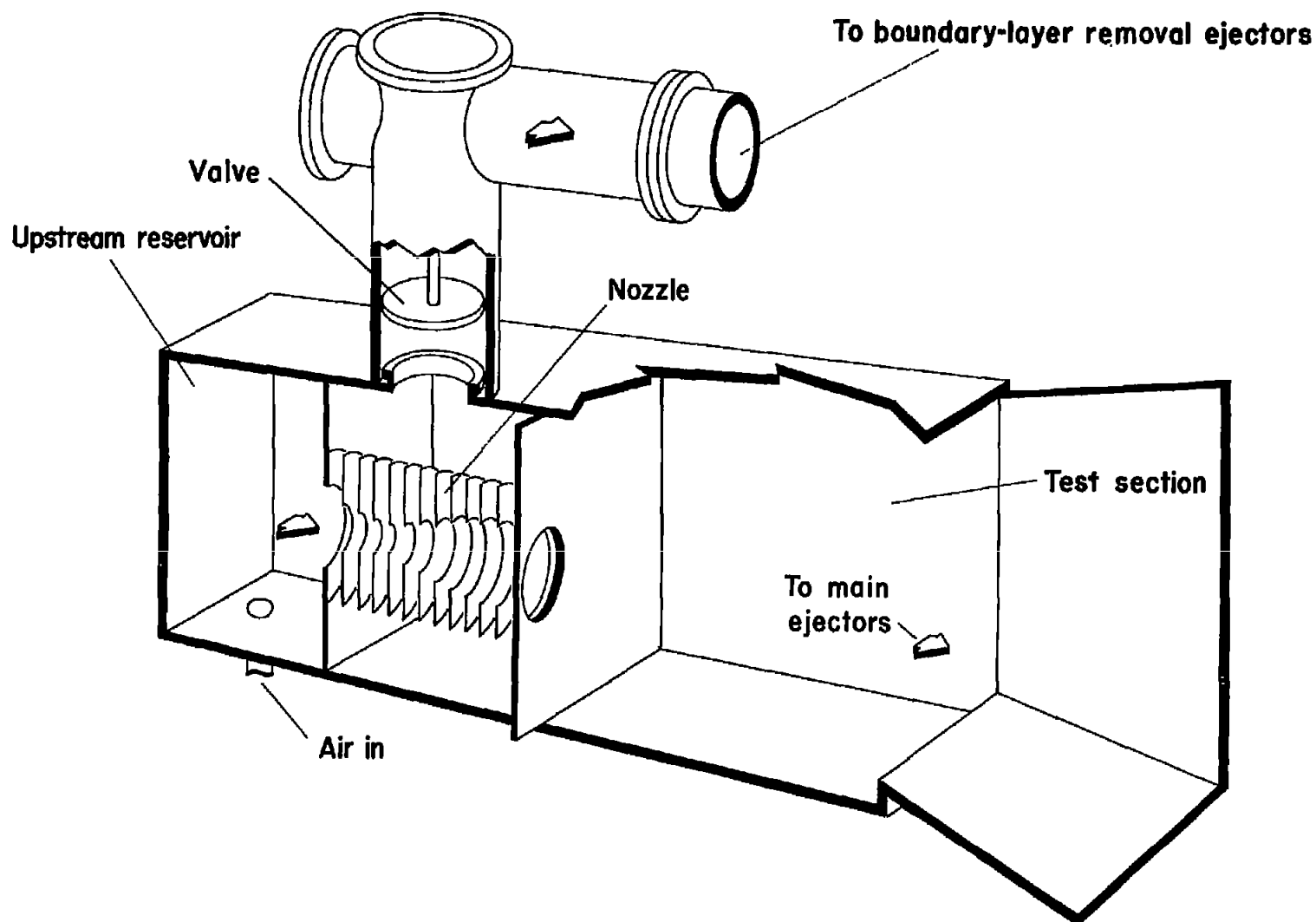
Figure 1.- General arrangement of wind-tunnel test section.
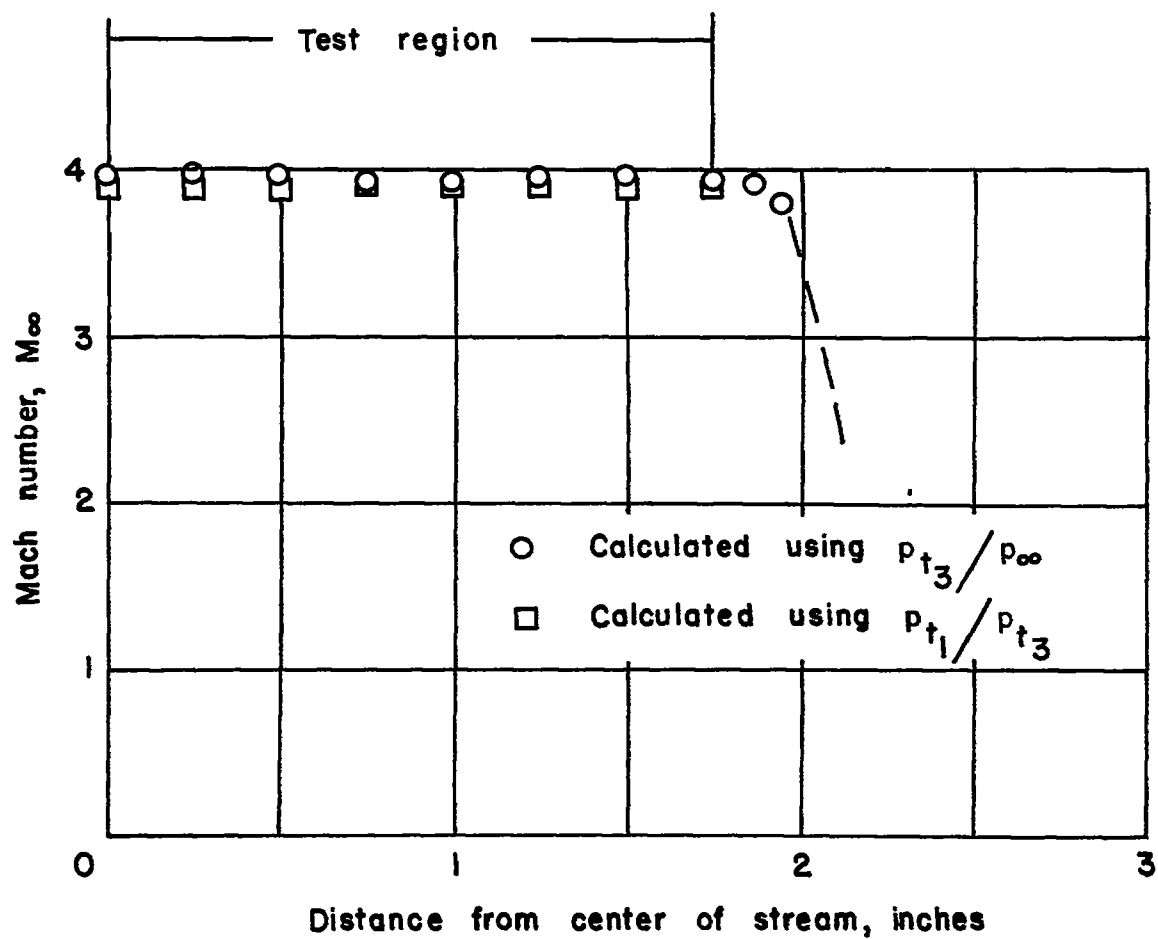
Figure 2.- Variation of Mach number with distance from center of stream for Reynolds number per inch of 6600 at axial distance of 1.25 inches from exit plane of nozzle.
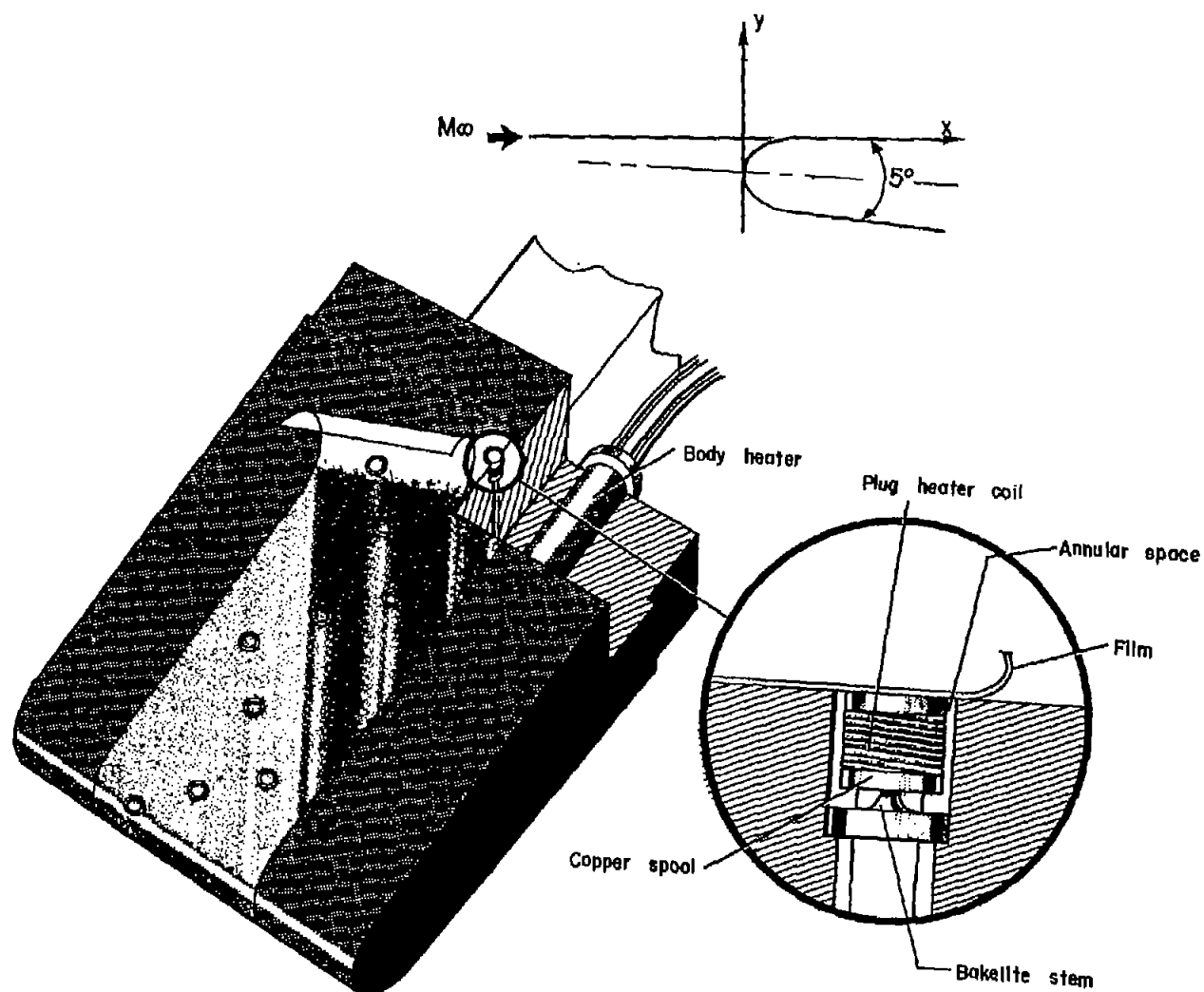
Figure 3.- Heat-transfer body.
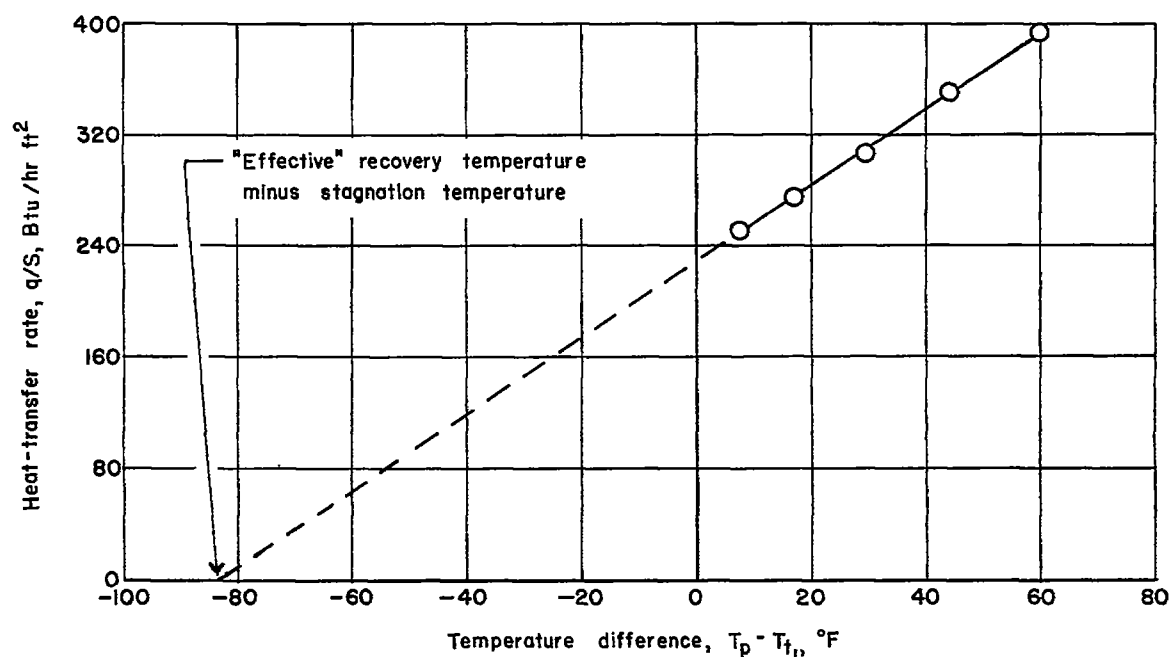
Figure 4.- Variation of heat-transfer rate with difference between surface temperature and stream stagnation temperature for free-stream conditions of $M_\infty = 3.95$ and $Re_{\infty d} = 6600.$
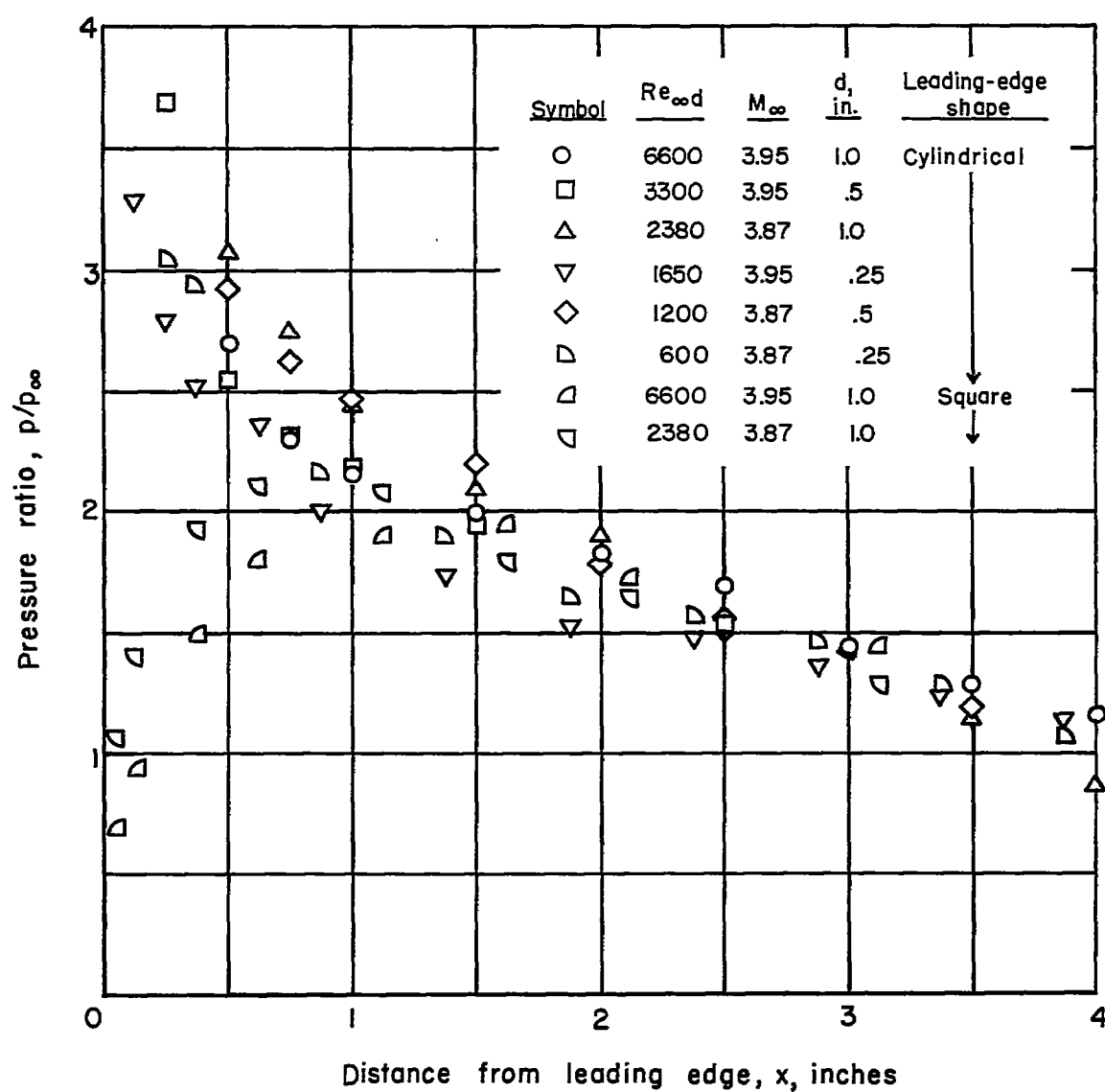
Figure 5.- Variation of the ratio of surface pressure to free-stream pressure with distance from the leading edge.
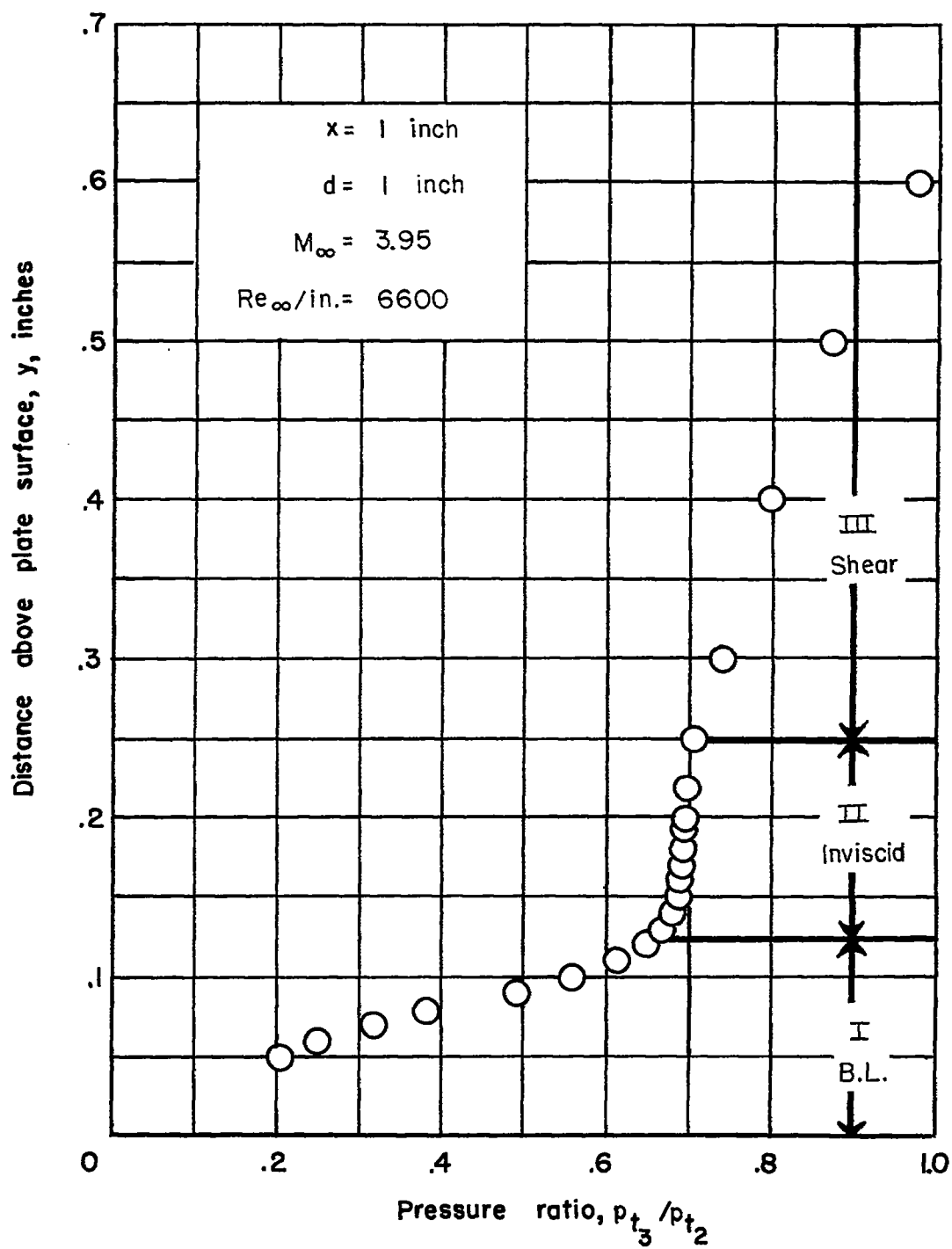
Figure 6.- Variation of the ratio of impact pressure to leading-edge
stagnation pressure with distance from the plate surface.
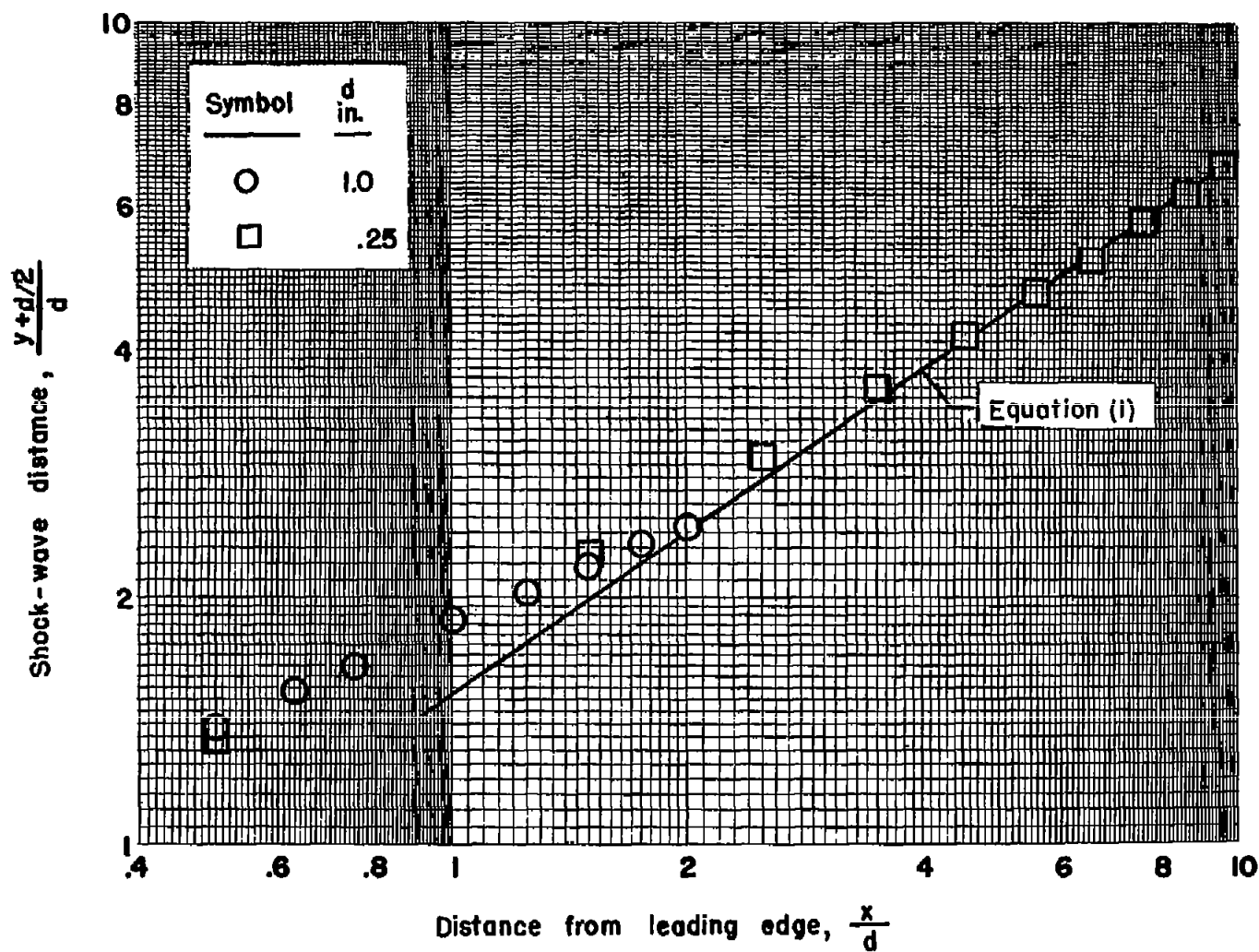
Figure 7.- Variation of shock-wave location with distance from leading
edge for $M_\infty = 3.95$ and Re_∞ per inch of 6600.
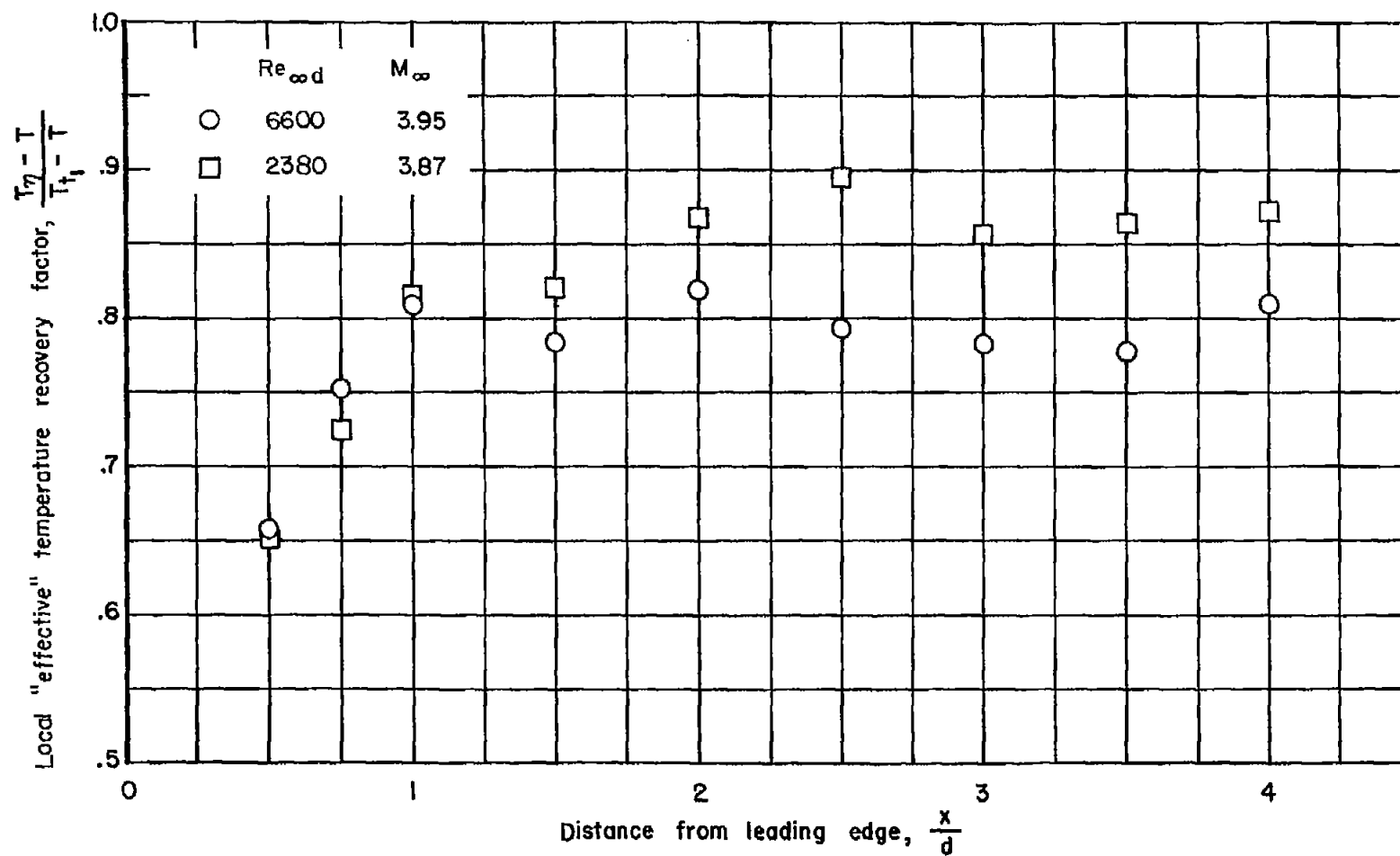
Figure 8.- Variation of the local "effective" temperature recovery factor with distance from the leading edge.
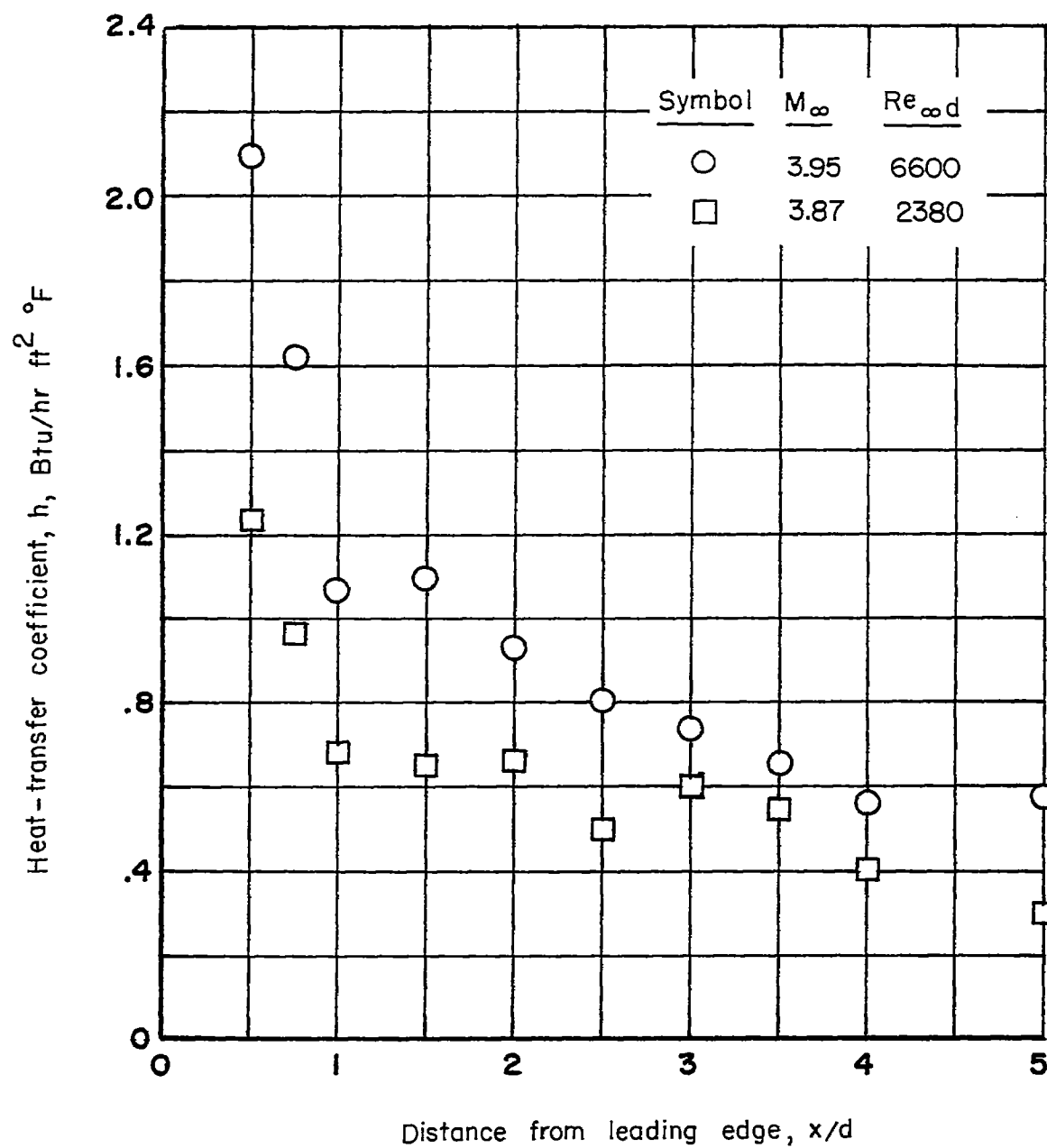
Figure 9.- Variation of heat-transfer coefficients with distance from
the leading edge.
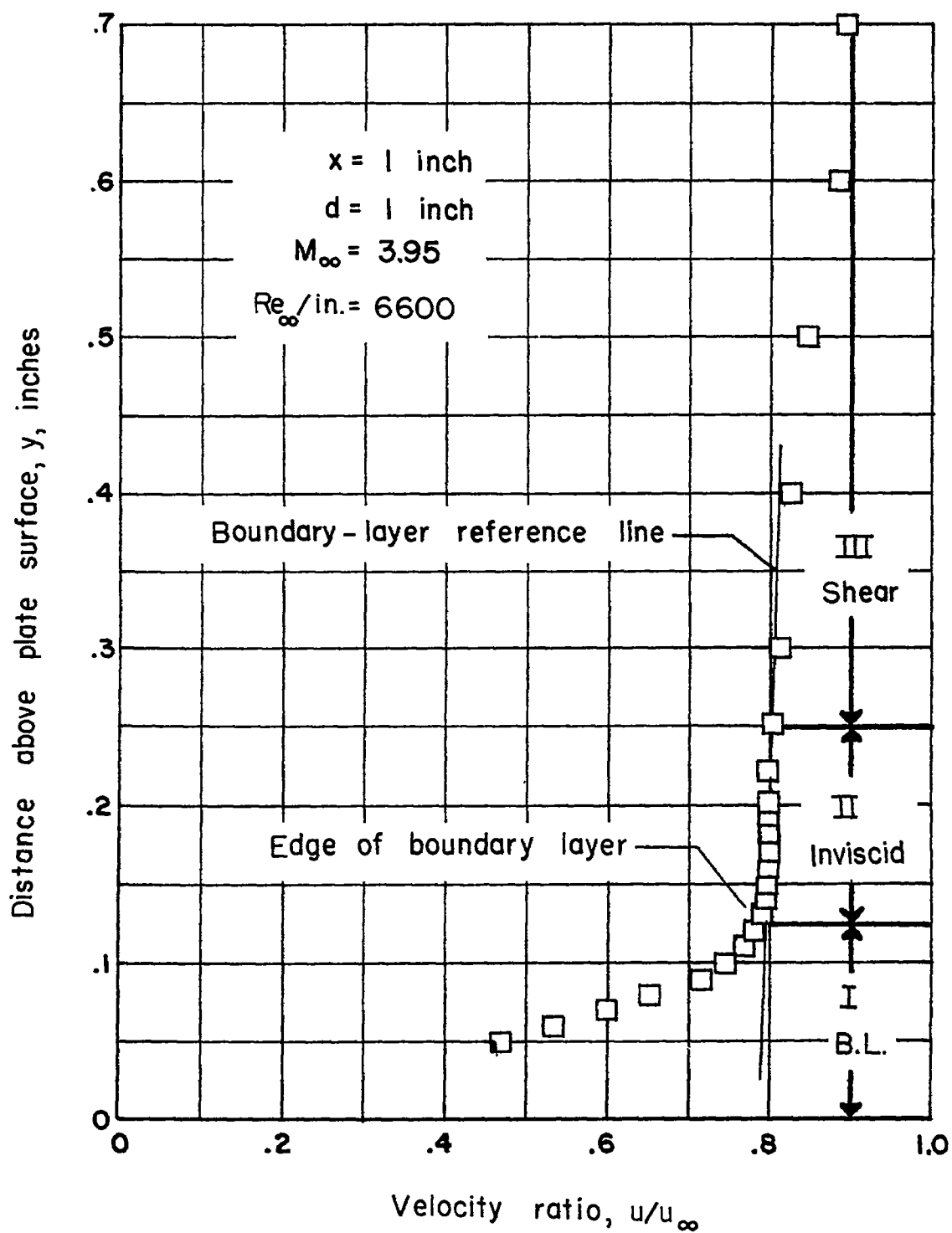
Figure 10.- Variation of the velocity ratio through the boundary layer.
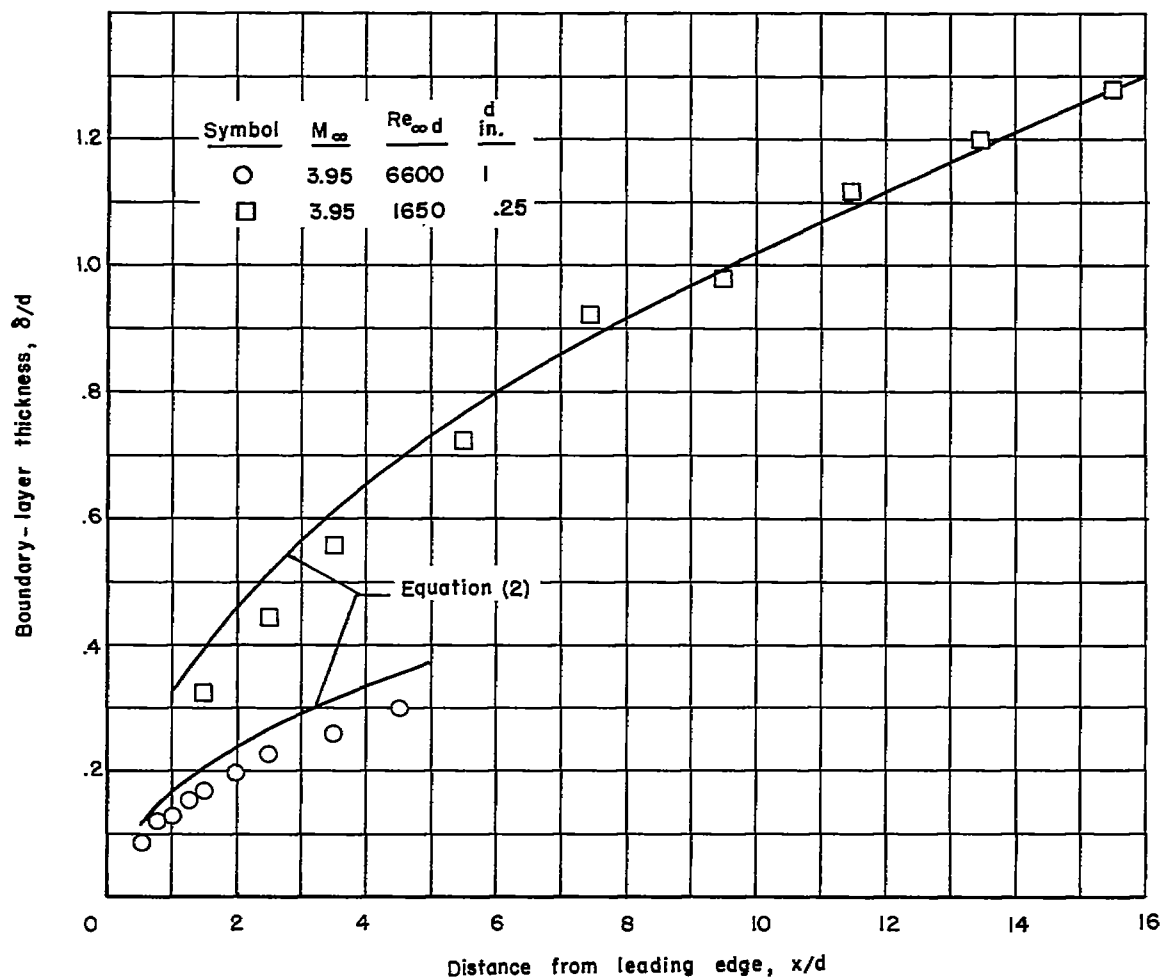
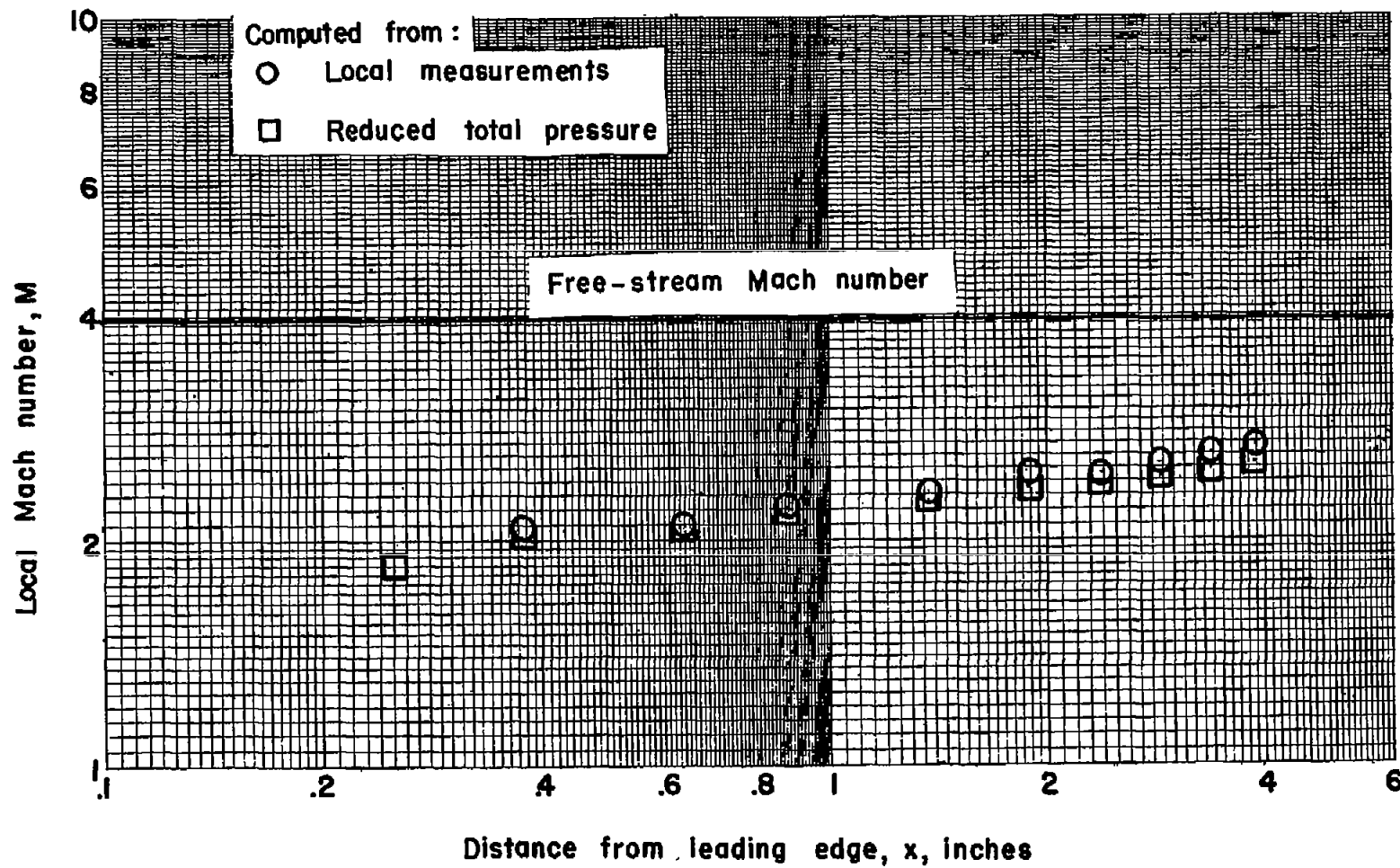Figure 11.- Comparison of measured boundary-layer thickness with theory.

Symbol	M_∞	Reference
○	3.9	Present tests
◻	5.8	Kendall
◇	6.86	Bertram
△	9.6	Bertram
▽	11.8	*HVB
◤	12.7	HVB
◁	16.0	Erickson
◌	17.3	Erickson

*Hammitt, Vas, and Bogdonoff
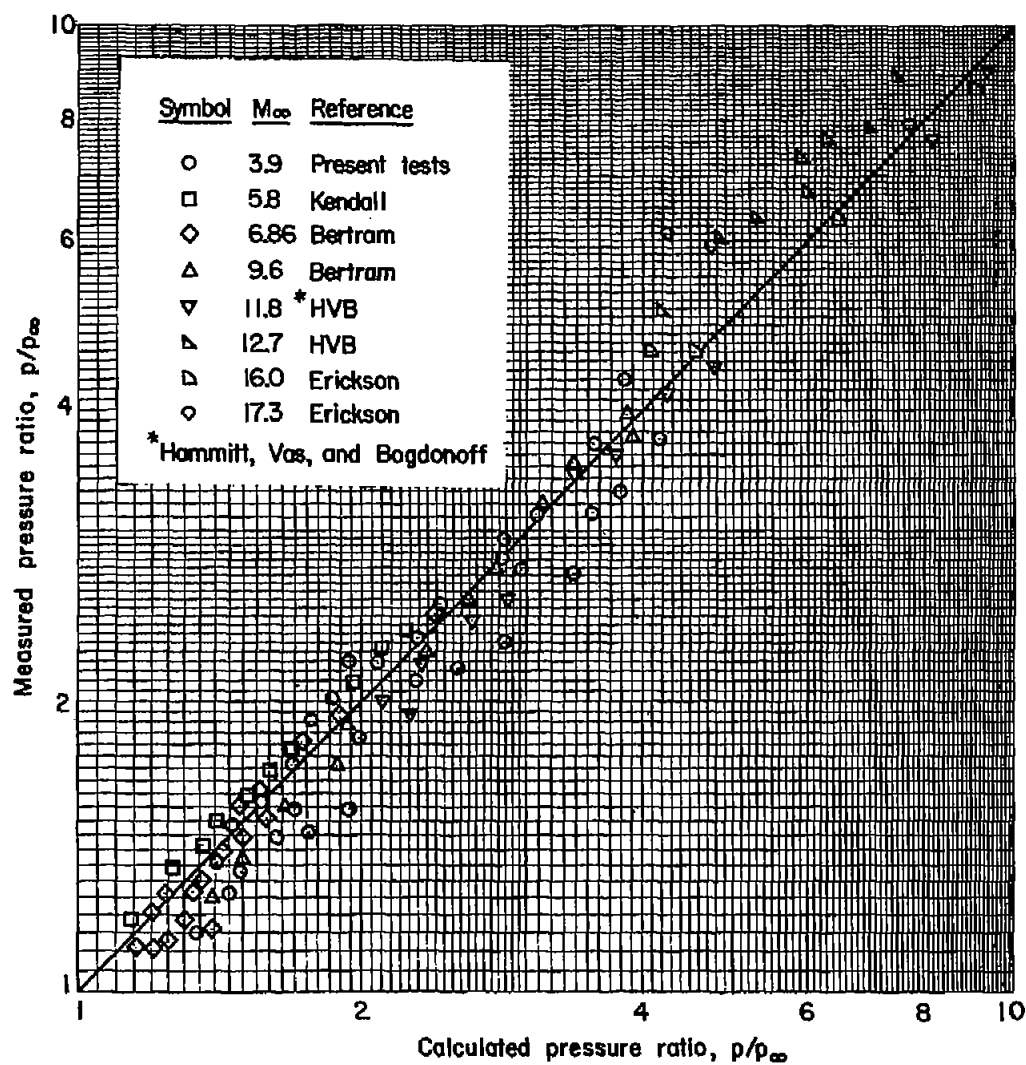
Figure 12.- Comparison of measured pressure ratios with calculated pressure ratios.

Distance from leading edge, x, inches
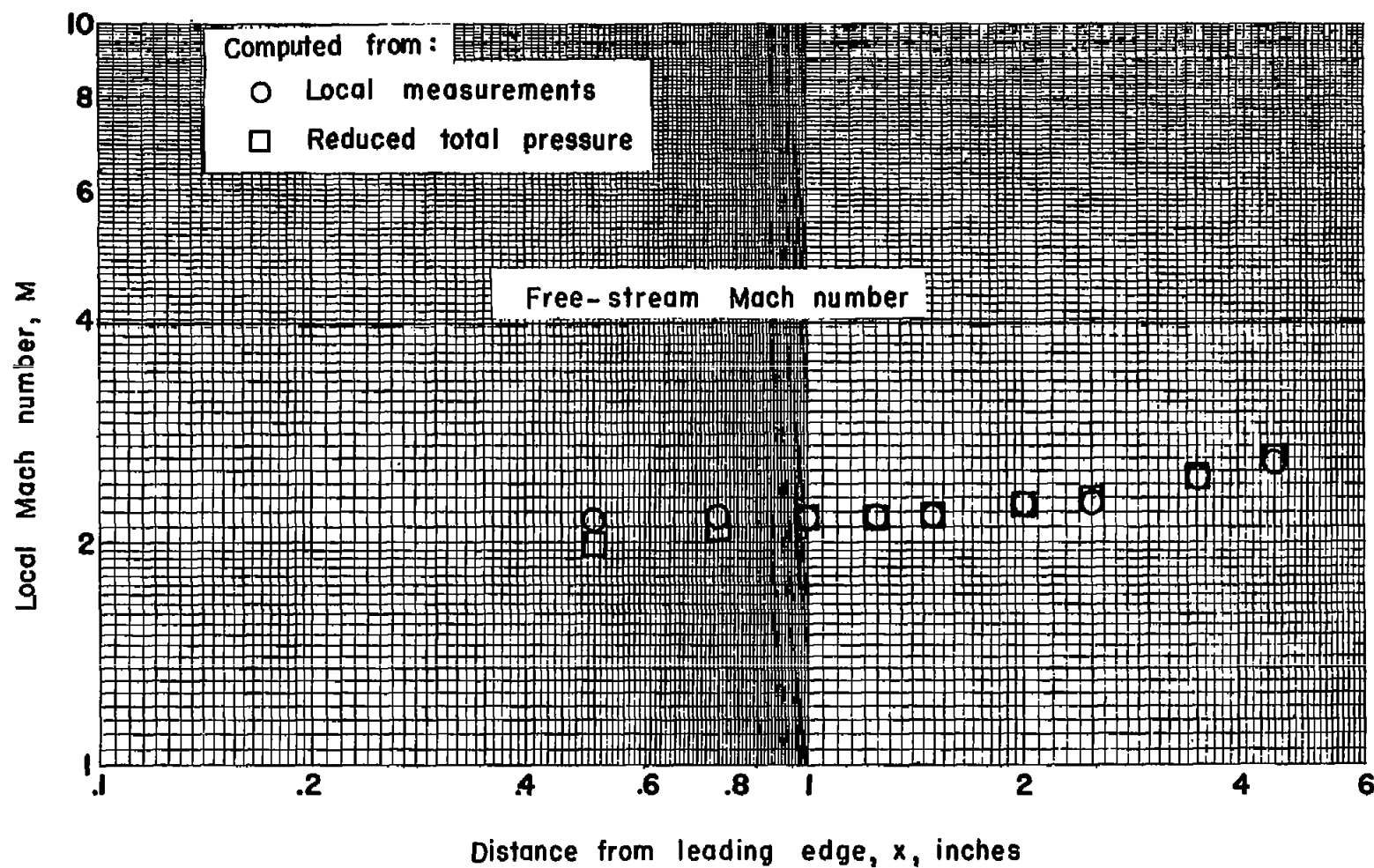
(a) $Re_{\infty d} = 6600$

Figure 13.- Variation of Mach number along the boundary-layer edge.

Distance from leading edge, x, inches

(b) $Re_{\infty d} = 1650$

Figure 13.- Concluded.

Symbol	d in.	M_∞	$Re_\infty d$	Leading-edge shape
o	1.0	3.95	6600	Cylindrical
□	.5		3300	
△	.25		1650	
◁	1.0	3.87	2380	
▷	.5		1190	
◻	.25		600	
◇	1.0	3.95	6600	Square
△	1.0	3.87	2380	
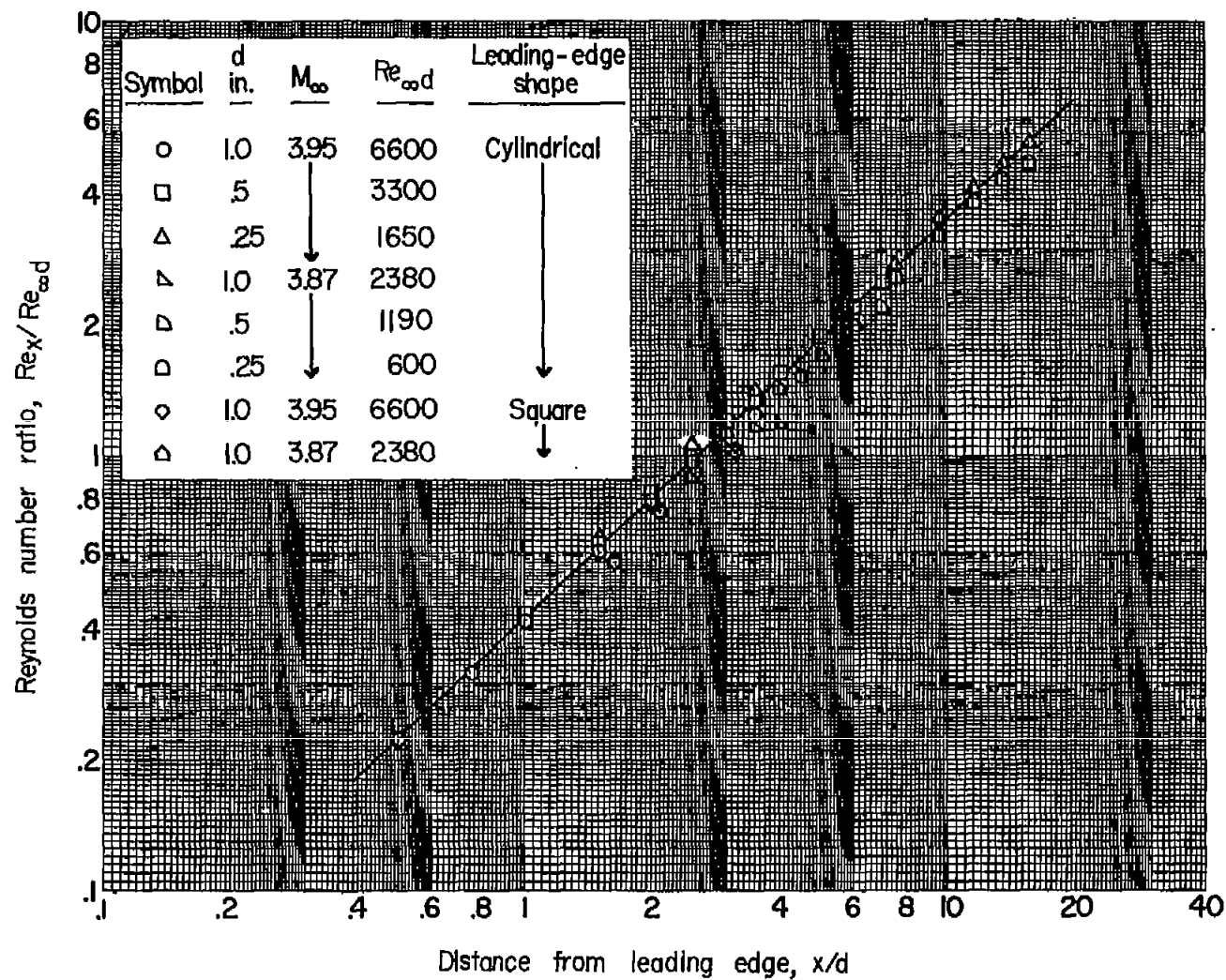
Figure 14.- Variation of the ratio of local Reynolds number at the boundary-layer edge to the free-stream Reynolds number with distance from the leading edge.
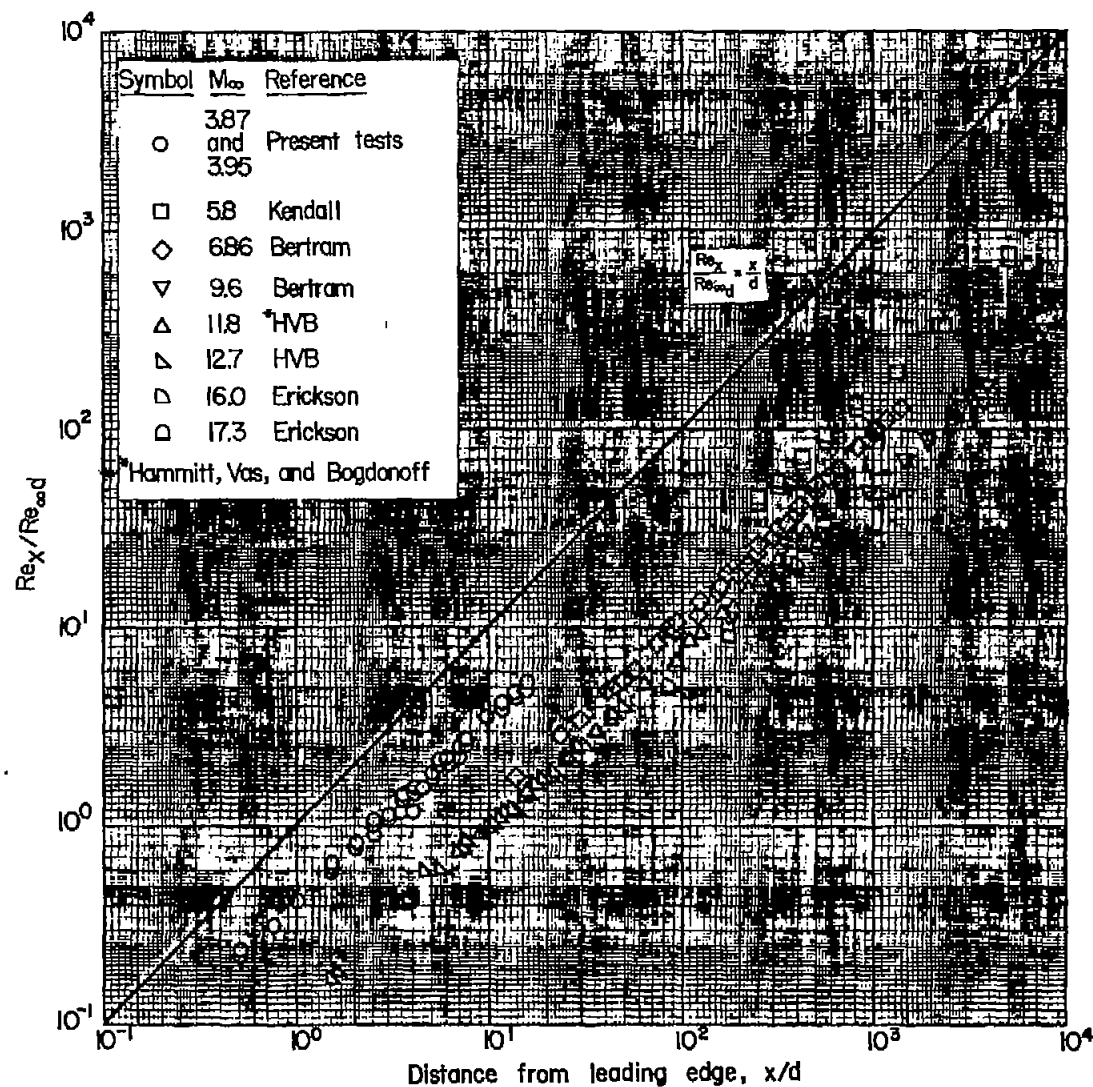
Figure 15.- Comparison of Reynolds number ratio from various sources, see table III.
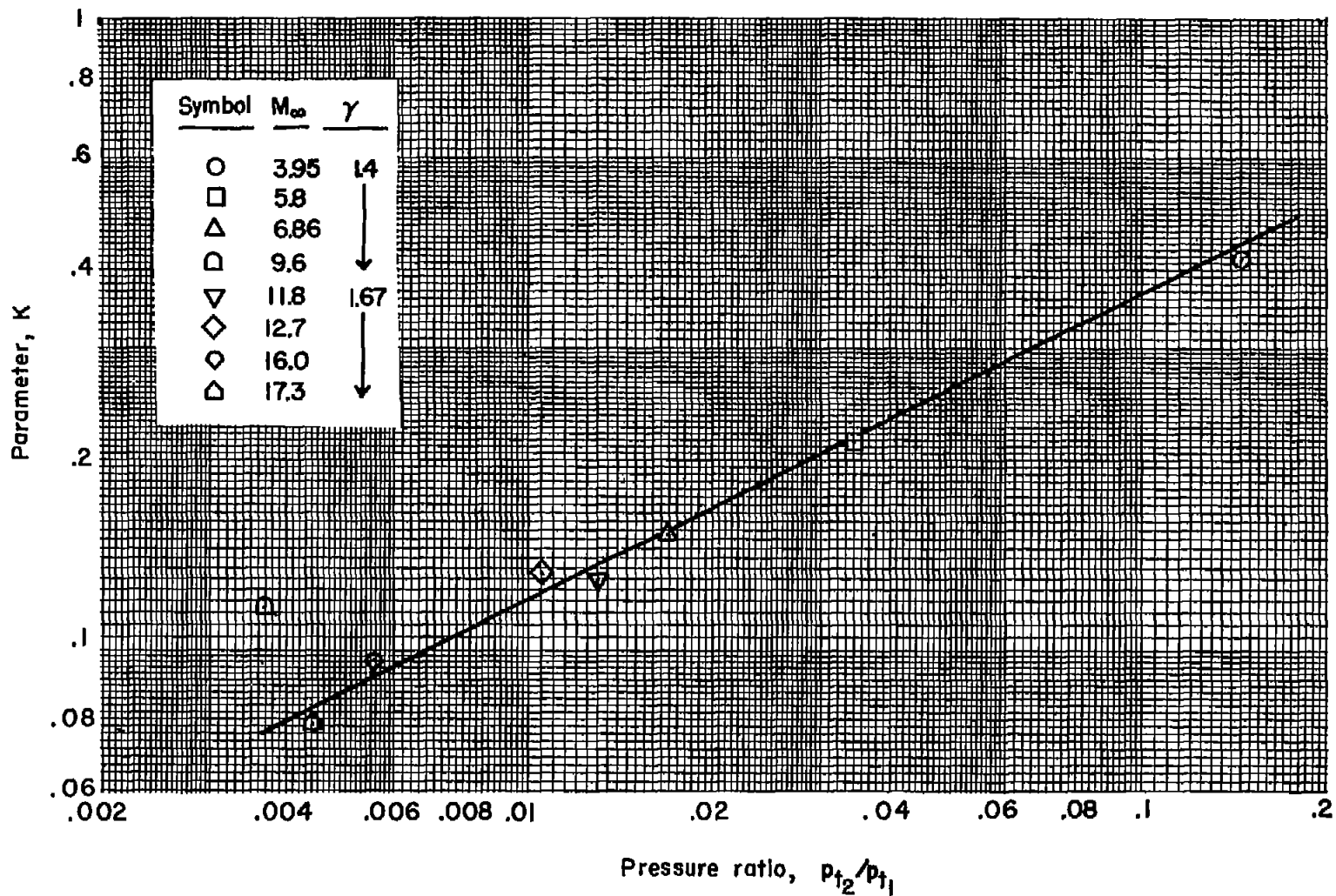
Figure 16.- Variation of the parameter K from various sources with total pressure ratio across a normal leading-edge shock wave.
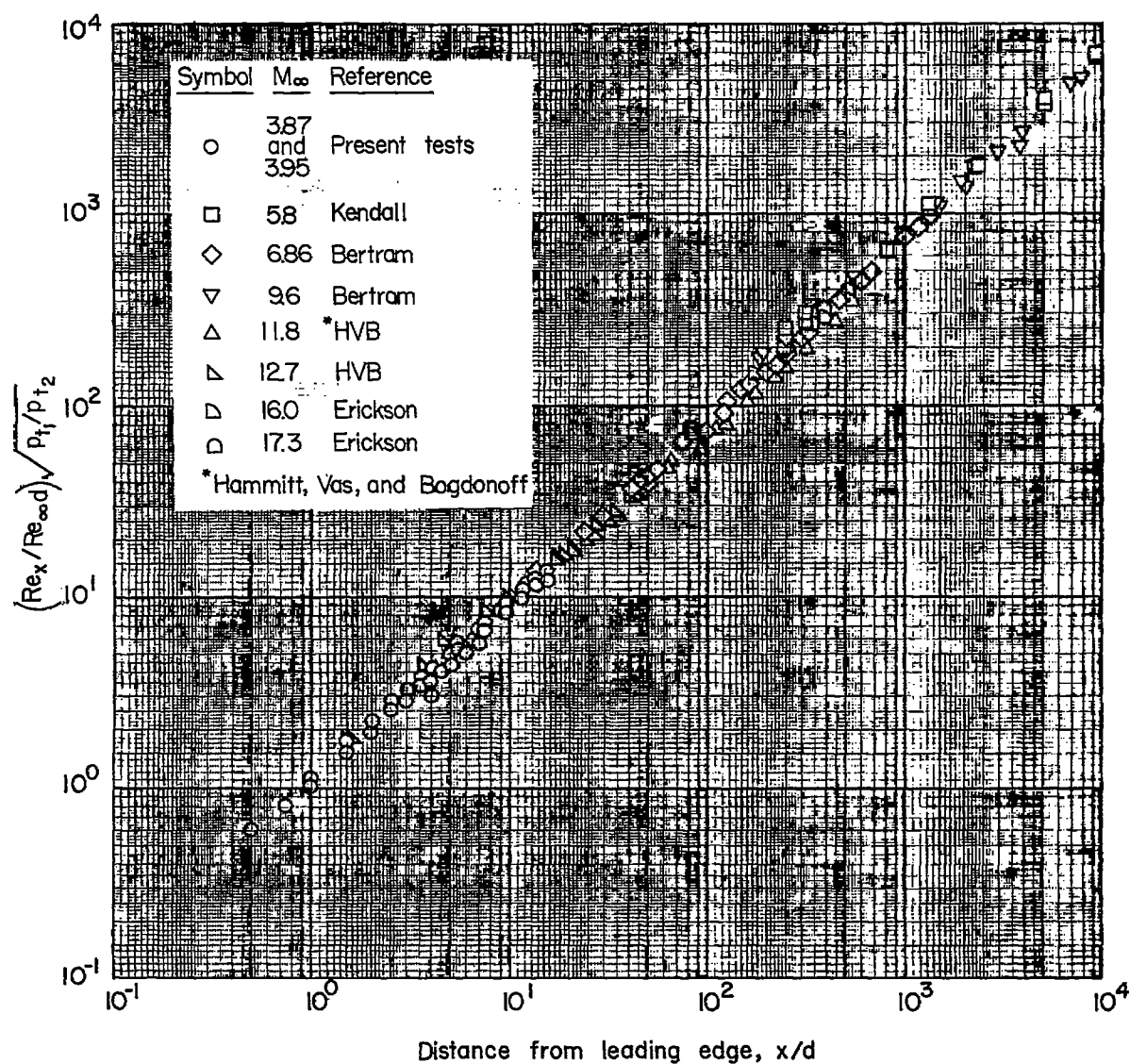
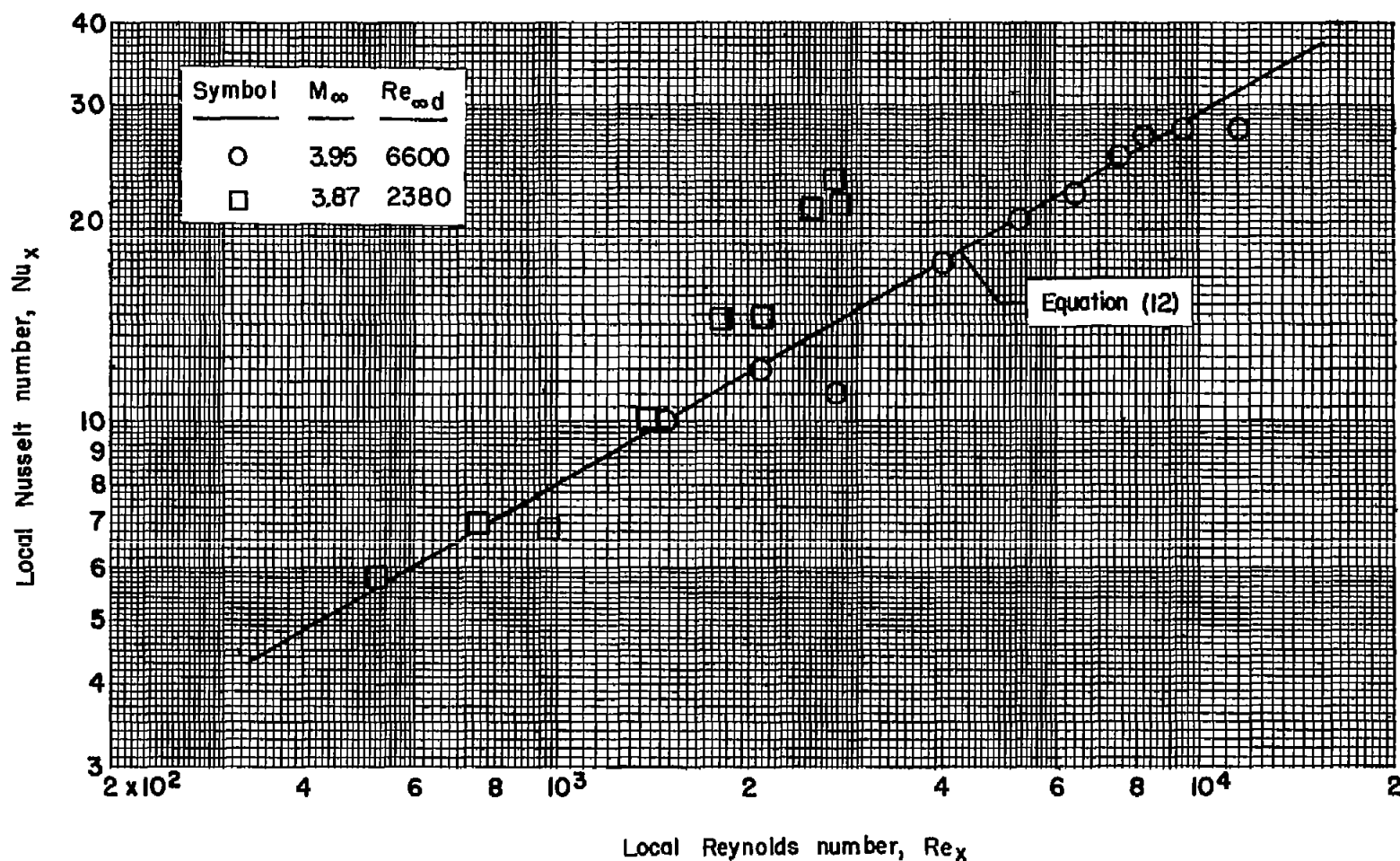Figure 17.- Correlation of results calculated from present tests and
from other sources.

Figure 18.- Variation of local Nusselt number with local Reynolds number for a cylindrically blunted flat plate in supersonic rarefied air flow.
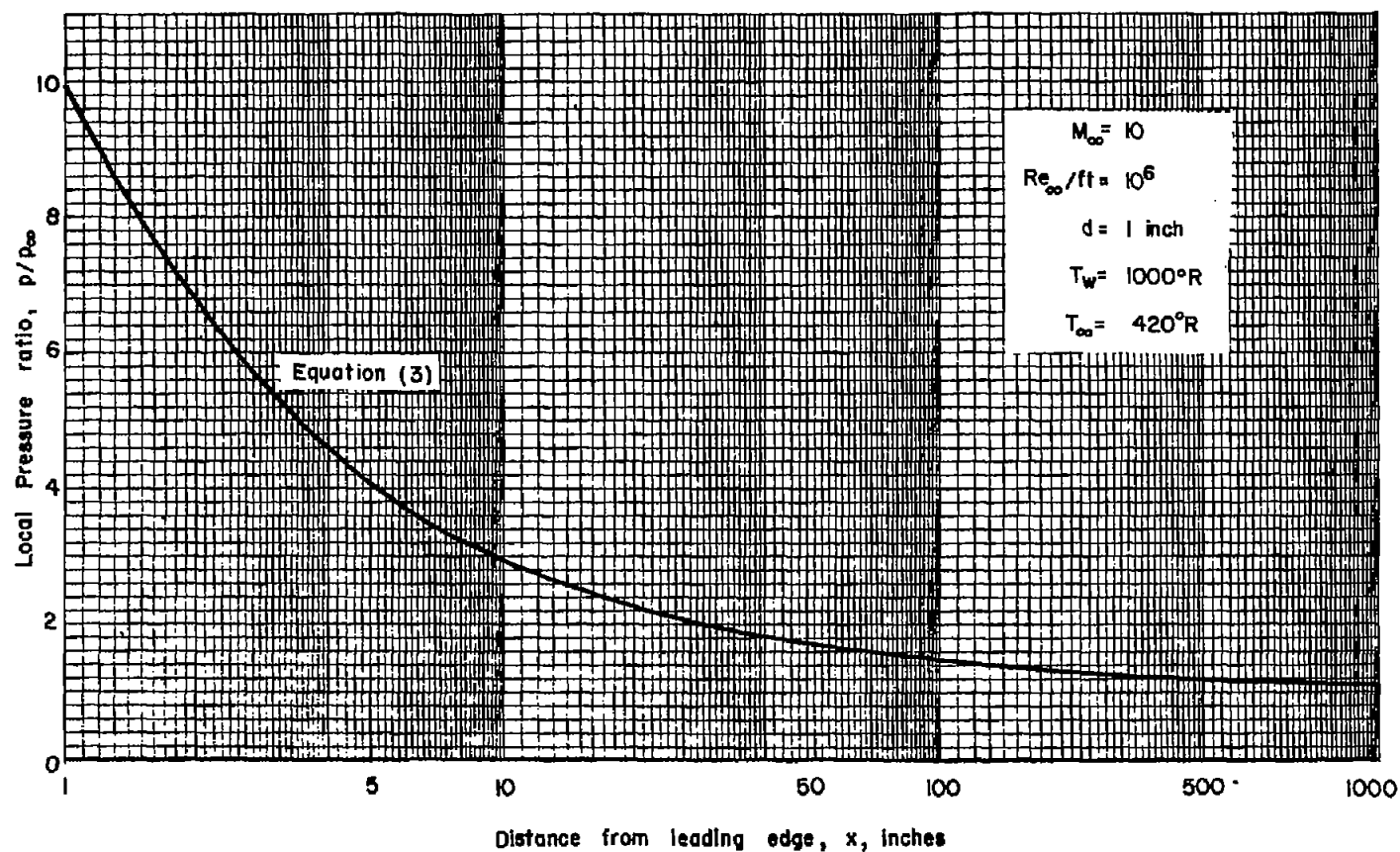
Figure 19.- Surface pressures calculated for a cylindrically blunted flat wing for zero angles of yaw and attack at an altitude of 100,000 feet.
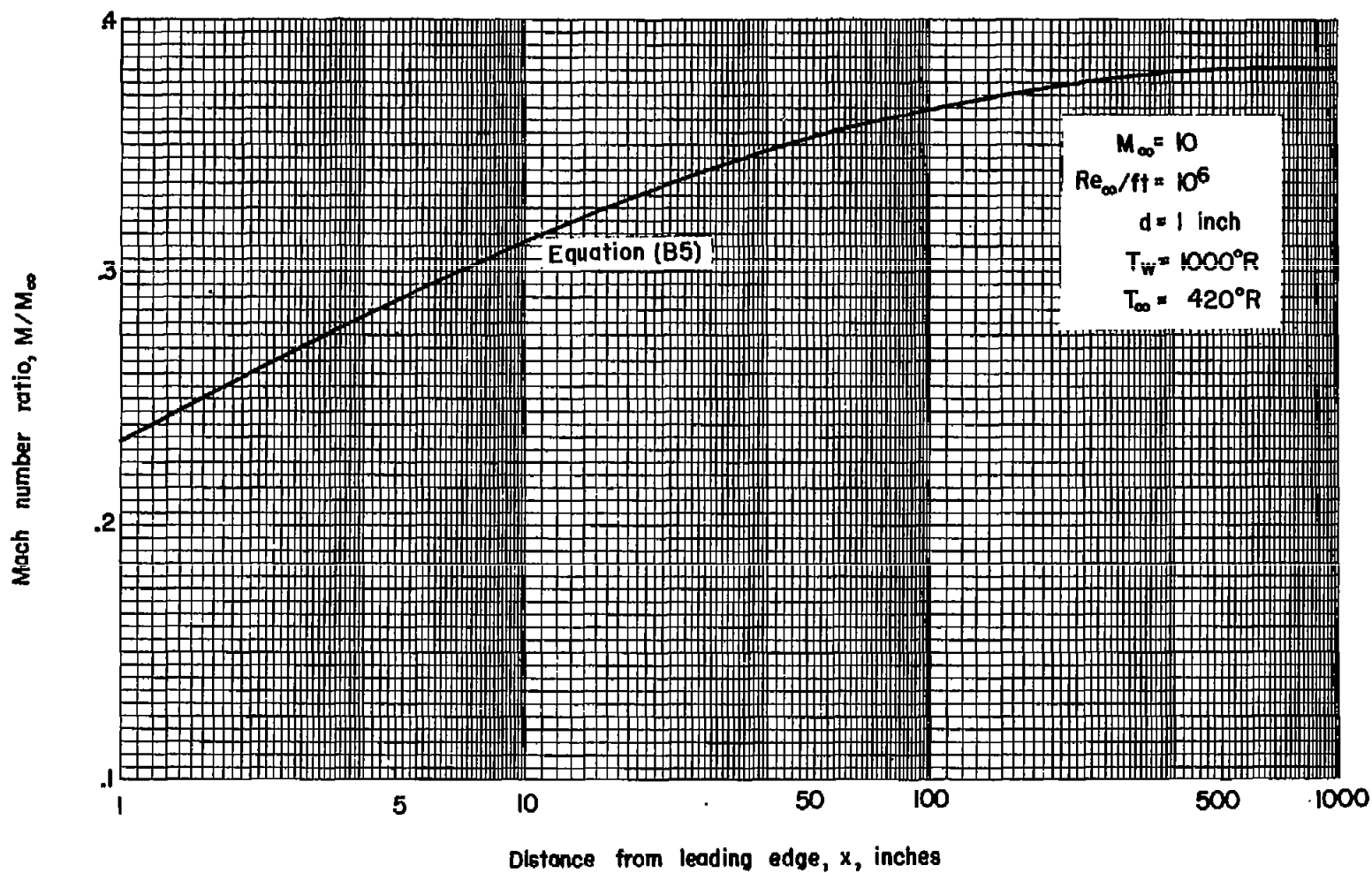
Figure 20.- Mach number ratio calculated for a cylindrically blunted flat wing for zero angles of attack and yaw at an altitude of 100,000 feet.
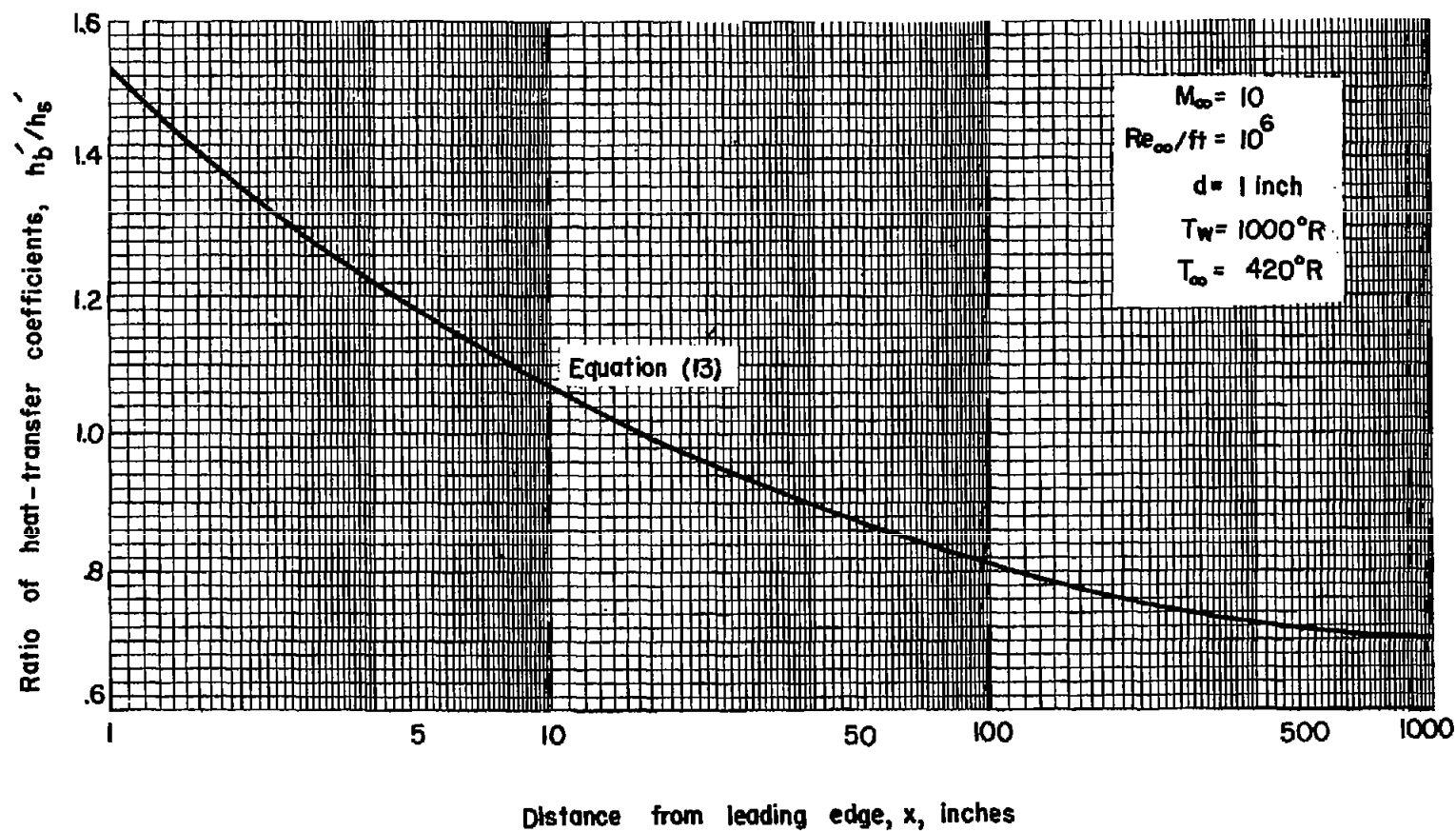
Figure 21.- Effect of blunting on the heat-transfer coefficients calculated for a flat wing for zero angles of attack and yaw at an altitude of 100,000 feet.